Novel Approaches to ECG-Based Modeling and Characterization of Atrial Fibrillation

Sandberg, Frida

2010

Novel Approaches to ECG-Based Modeling and Characterization of Atrial Fibrillation

Frida Sandberg

Lund 2010

Department of Electrical and Information Technology
Lund University
Box 118, SE-221 00 LUND
SWEDEN

This thesis is set in Computer Modern 10pt
with the LaTeX Documentation System

Series of licentiate and doctoral theses
No. 26
ISSN 1654-790X

Printed in Sweden by *Tryckeriet i E-huset*, Lund.
October 2010.

Till Peder, Emil och Arvid

Sammanfattning

Förmaksflimmer är den vanligaste rytmrubbningen i hjärtat som kräver behandling. Risken att drabbas ökar med åldern och 8% av alla åttioåringar lider av förmaksflimmer. Förmaksflimmer är i sig inte livshotande, men den förhöjda risken för proppbildning i förmaken kan leda till allvarliga komplikationer såsom stroke. Det finns olika behandlingsstrategier för förmaksflimmer, t.ex. medicinering, elkonvertering och kateterablation, men läkarna vet idag inte vilken metod som fungerar bäst för den enskilda patienten. Under förmaksflimmer är den elektriska aktiviteten i förmaken snabb och oregelbunden. De bakomliggande orsakerna till detta är inte fullständigt kartlagda. Ett enkelt och ofarligt sätt att studera den elektriska aktiviteten i hjärtat är genom elektrokardiogram (EKG), som mäts på kroppsytan.

Denna avhandling handlar om metoder för analys av EKG-signaler under förmaksflimmer. Målet är att kunna hjälpa läkare att fatta rätt beslut om behandling för den enskilda patienten. Egenskaper i EKG-signalen kan användas för att följa spontana förändringar i hjärtats elektriska aktivitet samt övervaka effekten av behandling. I vissa fall kan man även förutsäga effekten av en viss behandling för en enskild patient genom att analysera EKG-signalen.

I denna avhandling behandlas metoder för analys av förmakens aktivitet (artikel I–IV), och den elektriska kopplingen mellan förmak och kammare (artikel V) under förmaksflimmer. Under denna arytmi består EKG-signalen av flimmervågor, som avspeglar den elektriska aktiviteten i förmaken, och QRST komplex, som avspeglar den elektriska aktiviteten i kamrarna.

I artikel I används mått som kvantifierar olika egenskaper hos flimmervågorna, såsom amplitud, vågform, frekvens och komplexitet, för att undersöka skillnader mellan förmaksflimmer som upphör spontant och som ej upphör spontant. Det visar sig att flimmerfrekvensen kan användas för att förutspå spontan konvertering.

En ny metod för robust flimmerfrekvensanalys av långtids-EKG presenteras i artikel II, som bygger på en “hidden Markov modell” (HMM). Resultaten visar att frekvensestimaten är mer tillförlitliga än de som existerande metoder

producerar vid höga brusnivåer.

I artikel III används HMM-metoden för att analysera variationer i flimmerfrekvens över dygnet. Sådana cirkadiska variationer kan användas för att sätta in behandling vid en tidpunkt på dygnet då den bedöms ge störst effekt. Resultaten visar att flimmerfrekvensen i de flesta fall var högst under eftermiddagen, även om korttidsvariationen var betydande.

I artikel IV presenteras en entropi-baserad metod för analys av flimmervågor. Metoden kan användas för att skilja paroxysmalt (spontant konverterande) från persistent förmaksflimmer genom analys av 10-sekunders segment av långtids-EKG.

All överledning av elektriska impulser från förmaken till kamrarna går via AV-knutan. I artikel V presenteras en ny stokastisk modell för AV-knutans funktion under förmaksflimmer. Modellens parametrar kan estimeras från EKG-signalen. På så sätt kan egenskaper hos AV-knutan och förändringar hos dessa egenskaper kartläggas från EKG-signalen.

Abstract

This thesis deals with signal processing algorithms for analysis of the electrocardiogram (ECG) during atrial fibrillation (AF). Such analysis can be used for diagnosing patients, and for monitoring and predicting their response to various treatment. The thesis comprises an introduction and five papers describing methods for ECG-based modeling and characterization of AF. Paper I–IV deal with methods for characterization of the atrial activity, whereas Paper V deals with modeling of the ventricular response, both problems with the assumption that AF is present.

In Paper I, a number of measures characterizing the atrial activity in the ECG, obtained using time-frequency analysis as well as nonlinear methods, are evaluated for their ability to predict spontaneous termination of AF. The AF frequency, i.e, the repetition rate of the atrial fibrillatory waves of the ECG, proved to be a significant factor for discrimination between terminating and non-terminating AF.

Noise is a common problem in ECG signals, particularly in long-term ambulatory recordings. Hence, robust algorithms for analysis and characterization are required. In Paper II, a robust method for tracking the AF frequency in noisy signals is presented. The method is based on a hidden Markov model (HMM), which takes the harmonic pattern of the atrial activity into account. Using the HMM-based method, the average RMS error of the frequency estimates at high noise levels was significantly lower compared to existing methods.

In Paper III, the HMM-based method is employed for analysis of 24-h ambulatory ECG signals in order to explore circadian variation in AF frequency. Circadian variations reflect autonomic modulation; attenuation or absence of such variations may help to diagnose patients. Methods based on curve fitting, autocorrelation, and joint variation, respectively, are employed to quantify circadian variations, showing that it is present in most patients with long-standing persistent AF, although the short-term variation is considerable.

In Paper IV, 24-h ambulatory ECG recordings with paroxysmal and persistent AF are analyzed using an entropy-based method for characterization

of the atrial activity. Short segments are classified based on these measures, showing that it is feasible to distinguish between patient with paroxysmal and persistent AF from 10-s ECGs; the average classification rate was above 95%.

The ventricular response during AF is mainly determined by the AV nodal blocking of atrial impulses. In Paper V, a new model-based approach for analysis of the ventricular response during AF is proposed. The model integrates physiological properties of the AV node and the atrial fibrillatory rate; the model parameters can be estimated from ECG signals. Results show that ventricular response is sufficiently represented by the estimated model in a majority of the recordings; in 85.7% of the analyzed 30-min segments the model fit was considered accurate, and that changes of AV nodal properties caused by autonomic modulation could be tracked through the estimated model parameters.

In summary, the work within this thesis contributes with new methods for non-invasive analysis of AF, which can be used to tailor and evaluate different strategies for AF treatment.

Preface

This doctoral thesis comprises an introduction and five parts describing signal processing methods for modeling and characterization of atrial fibrillation from the ECG. The parts are based on the following journal papers:

[1] Frida Nilsson, Martin Stridh, Andreas Bollmann, and Leif Sörnmo, "Predicting spontaneous termination of atrial fibrillation using the surface ECG," *Medical Engineering & Physics*, vol. 28, pp. 802–808, 2006. **(This paper was among the top 10 cited during 2006–2008 in the journal.)**

[2] Frida Sandberg, Martin Stridh and Leif Sörnmo, "Frequency tracking of atrial fibrillation using hidden Markov models," *IEEE Transactions on Biomedical Engineering*, vol. 55, pp. 502–511, 2008.

[3] Frida Sandberg, Andreas Bollmann, Daniela Husser, Martin Stridh and Leif Sörnmo, "Circadian variation in dominant atrial fibrillation frequency in persistent atrial fibrillation," *Physiological Measurement*, vol. 31, pp. 531–542, 2010.

[4] Raúl Alcaraz, Frida Sandberg, Leif Sörnmo, and José Joaquín Rieta, "Classification of paroxysmal and persistent atrial fibrillation in ambulatory ECG recordings," Submitted for publication.

[5] Frida Sandberg, Valentina Corino, Luca Mainardi and Leif Sörnmo, "Model-based analysis of the ventricular response during atrial fibrillation," Manuscript.

In Paper I–III, the author of this thesis performed the analysis, developed and/or evaluated the methods and prepared the manuscripts. In Paper IV–V, the development of the methods, the analysis and the manuscript was to equal parts conducted by the author and the collaborating group. Different parts of the work have also been presented in various contexts:

[6] Frida Sandberg, Martin Stridh and Leif Sörnmo, "Time-frequency analysis of atrial fibrillation," in *Understanding Atrial Fibrillation: The Signal Processing Contribuiton*, L. Mainardi, L. Sörnmo, and S. Cerutti (eds), Morgan & Claypool Publ., pp 81–102, 2008.

[7] Frida Nilsson, Martin Stridh and Leif Sörnmo, "Comparison of Spectral Properties in Atrial Signals Using Different QRST Cancellation Techniques," in *Proc. IFMBE*, Ischia, Italy, vol. 6, Aug. 2004.

[8] Frida Nilsson, Martin Stridh, Andreas Bollmann, and Leif Sörnmo, "Predicting spontaneous termination of atrial fibrillation with time-frequency information," in *Proc. Computers in Cardiology*, Chicago, USA, vol. 31, pp. 657–660, Sept. 2004.

[9] Frida Nilsson, Martin Stridh and Leif Sörnmo, "Frequency tracking of atrial fibrillation using hidden Markov models," in *Proc. 28th Annual International Conference of the IEEE Engineering in Medicine and Biology Society, EMBS '06.*, New York, USA, pp. 1406–1409, Sept. 2006.

[10] Frida Sandberg, Andreas Bollman, Daniela Husser, Martin Stridh and Leif Sörnmo, "Quantitative analysis of circadian variation in atrial fibrillation frequency", in *Proc. Computers in Cardiology*, Park City, USA, vol. 36, pp. 129–132, Sept. 2009.

[11] Raúl Alcaraz, Frida Sandberg, Leif Sörnmo and José Joaquín Rieta, "Organization tracking of long-term atrial fibrillation recordings: Differences between paroxysmal and persistent episodes" in *Proc. Computers in Cardiology*, Park City, USA, vol. 36, pp. 509–512, Sept. 2009.

[12] Frida Sandberg, Raúl Alcaraz, José Joaquín Rieta and Leif Sörnmo, "Non-invasive estimation of organization evidences differences between paroxysmal and persistent AF" *International Congress on Electrocardiology 2010*, Lund, Sweden, June 2010.

[13] Frida Sandberg, Valentina Corino, Luca Mainardi and Leif Sörnmo, "Ventricular response during AF – A mathematical model of the AV nodal function" *International Congress on Electrocardiology*, Lund, Sweden, June 2010.

[14] Richard Petersson, Frida Sandberg, José Joaquín Rieta, Raúl Alcaraz, Pyotr Platonov and Fredrik Holmqvist, "Non-invasive estimation of organization in atrial fibrillation as a predictor of sinus rhythm maintenance" *International Congress on Electrocardiology*, Lund, Sweden, June 2010.

[15] Raúl Alcaraz, Frida Sandberg, Leif Sörnmo and José Joaquín Rieta, "Application of frequency and sample entropy to discriminate long-term recordings of paroxysmal and persistent atrial fibrillation" in *Proc. 32th Annual International Conference of the IEEE Engineering in Medicine and Biology Society, EMBS '10.*, Buenos Aires, Argentina, Sept. 2010. **(invited paper)**

[16] Valentina Corino, Frida Sandberg, Leif Sörnmo and Luca Mainardi, "A mathematical model of atrioventricular node during atrial fibrillation" in *Proc. Computing in Cardiology*, Belfast, Northern Ireland, Sept. 2010.

Acknowledgments

I would like to take the opportunity to acknowledge those who have made my time working on this thesis a true pleasure.

First I would like to express my gratitude to my supervisor, Prof. Leif Sörnmo, for sharing his knowledge and experience with me, and for supporting and encouraging me during these years. He was the one that introduced me to the field of biomedical signal processing, and his catching enthusiasm was the reason I started my postgraduate studies.

I am also grateful to my co-supervisor Dr. Martin Stridh, for all his help and support. His expertise on signal processing of atrial fibrillation ECGs gave me a head start on my work.

I would like to thank Ulrike Richter, Kristian Solem, Danny Smith, and the rest of the signal processing group for interesting discussions and valuable help. A special thanks to Ulrike for creating such a nice atmosphere in our room. I really enjoyed our conversations across the table.

I have very much appreciated the interesting discussions and fruitful collaborations with Raúl Alcaraz and José Joaquín Rieta in Valencia, Spain, and Valentina Corino and Luca Mainardi in Milan, Italy. I particularly enjoyed the intense Skype conversations with Vale.

Being an engineer working this field, I rely on the medical expertise of others. Therefore I would like to thank Andreas Bollmann, Daniela Husser and the staff at the Dept. of Cardiology, Lund University, for their valuable input.

I also wish to thank my other colleges and friends at the Dept. of Electrical and Information Technology, for the nice company and all the interesting and entertaining discussions during coffee breaks and lunches. This is what makes it fun to go to work every morning.

Thanks also to the technical and administrative staff at the Dept. of Electrical and Information Technology for all help with practical issues.

Finally, I'm grateful to my friends and family for always supporting me. Thanks to my parents, Solgerd and Lars-Börje, for your help while I was work-

ing on this thesis. Thank you Peder for all your patience, love and support. You and Emil and Arvid make me so happy.

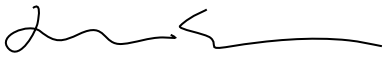

Frida Sandberg

List of Acronyms and Abbreviations

AF Atrial Fibrillation

AROC Area under ROC curve

AV Atrioventricular

BSPM Body Surface Potential Mapping

CWD Choi–Williams Distribution

ECG Electrocardiogram

HMM Hidden Markov Model

HRSH Heart Rate Stratified Histogram

ICA Independent Component Analysis

PA Paroxysmal

PCA Principal Component Analysis

PDF Probability Density Function

PE Persistent

PRSA Phase-Rectified Signal Averaging

PSP Poincaré Surface Profile

RMS Root Mean Square

ROC Region of Convergence

SNR Signal-to-Noise Ratio

SPA Second Peak Amplitude

SPP Second Peak Position

STD Standard Deviation

STFT Short-Time Fourier Transform

SVD Singular Value Decomposition

XWVD Cross Wigner–Ville Distribution

Contents

Part I

Overview of the Research Field

Chapter 1

Introduction

This thesis deals with signal processing algorithms for analysis of the electrocardiogram (ECG) during atrial fibrillation (AF). Atrial fibrillation is one of the most common cardiac arrhythmias in clinical practice. Although it is not life-threatening, it is associated with higher mortality in the long-term perspective. The underlying mechanisms of AF are not completely known but are currently subject to intense research. Various strategies for treatment have been proposed but none has been found as optimal for all patients.

The surface ECG reflects the global electrical activity of the heart. Although the local and complex impulse propagation pattern in the atria during AF cannot be studied in detail from the ECG, it offers possibilities for safe and inexpensive monitoring of the cardiac activity. Various aspects of the unorganized atrial activity and the irregular ventricular response during AF can be explored by examination of the ECG signal. Since manual inspection of ECG signals is time-consuming and subjective, methods for automatic analysis of the atrial and ventricular activity in the ECG during AF are essential. Features extracted from the ECG characterizing AF, may be used as a basis for selection of patient therapy and for noninvasive monitoring of the effects of treatment.

There are several challenges when analyzing AF from the ECG. A general problem in biomedical signal processing is that the exact properties of the underlying physiological processes causing the signals are not known. Hence, there is no 'gold standard' that can be used for evaluation of different analysis methods, but the performance can only be evaluated indirectly. One way to evaluate a method is by verifying the clinical relevance of the extracted features by, e.g., their ability to separate different patient groups, monitor effects, or predict treatment outcome. The repetition rate of the atrial fibrillator waves in the ECG has been found to correlate well with the invasively measured atrial

cycle length. Other characteristics of the atrial activity, e.g., morphology and complexity, may reflect different properties of the propagation of impulses in the atria. Hence, methods for quantification of these characteristics are needed. A problem when analyzing AF in the ECG is that the ventricular activity has much larger magnitude than does the atrial activity. To perform detailed analysis of the atrial activity, the ventricular activity needs to be cancelled. Since atrial and ventricular activity temporally and spectrally overlap, simple filtering approaches are not sufficient. Noise is a common problem in ECG signals, particularly in long-term ambulatory recordings. Whereas some types of noise, e.g., 50/60 Hz power line interference, can easily be removed by filtering the ECG, other types of noise, e.g., muscular artifacts, are more difficult to eliminate. Methods for analysis and characterization of atrial activity are therefore required to be robust to such noise. The ventricular response during AF is mainly determined by the atrioventricular (AV) node. Characteristics of the series of ventricular inter-activation times derived from the ECG can therefore be used to explore AV nodal properties. Hence, methods for modeling and characterization of the ventricular response during AF are needed.

Paper I–IV deals with characterization of atrial activity during AF, while Paper V mainly deals with characterization of the ventricular response. In Paper I, a number of measures characterizing the atrial activity in the ECG, obtained using time-frequency analysis as well as nonlinear methods, are evaluated for their ability to predict spontaneous termination of AF. The AF frequency, i.e, the repetition rate of the atrial fibrillatory waves of the ECG, proved to be a significant factor for discrimination between terminating and non-terminating AF.

In Paper II, a robust method for tracking the AF frequency in noisy ECG signals is presented. The method is based on a hidden Markov model (HMM), which takes the harmonic pattern of the atrial activity into account. Using the HMM-based method, the average RMS error of the frequency estimates at high noise levels was significantly lower compared to existing methods.

In Paper III, the HMM-based method is employed for analyzing 24-h ambulatory ECG signals in order to explore circadian variation in AF frequency. Circadian variations reflect autonomic modulation; absence of such variations may help to diagnose patients. Methods based on curve fitting, autocorrelation, and joint variation, respectively, are employed to quantify circadian variations, showing that it is present in most patients with long-standing persistent AF, although the short-term variation are considerable.

In Paper IV, 24-h ambulatory ECG recordings with paroxysmal and persistent AF are analyzed using an entropy-based method for characterizing the atrial activity. Short segments are classified based on these measures, showing that it is feasible to distinguish between patient with paroxysmal and persistent

AF from 10-s ECGs; the average classification rate was above 95%.

In Paper V, a new model-based approach for analysis of the ventricular response during AF is proposed. The model integrates physiological properties of the AV node and the atrial fibrillatory rate; the model parameters can be estimated from ECG signals. Results show that ventricular response is sufficiently represented by the estimated model in a majority of the recordings; in 85.7% of the analyzed 30-min segments the model fit was considered accurate, and that changes of AV nodal properties caused by autonomic modulation could be tracked through the estimated model parameters.

A short background to AF and ECG signals is given in Chapter 2. Chapter 3 deals with the issue of extracting atrial activity from the ECG during AF. In Chapter 4, different methods for characterization of the atrial activity of the ECG during AF are presented, whereas Chapter 5 deals with methods for analysis and modeling of the ventricular response during AF. A summary of the included papers is found in Chapter 6.

Chapter 2

Atrial Fibrillation

2.1 The Normal Heart

The heart is divided into a left and a right part, each consisting of two chambers; the atrium and the ventricle [1], see Fig. 2.1. The two parts are divided by a muscular wall, called septum. Different valves control the direction of the blood flow; the atrioventricular valves between the atria and the ventricles, and the pulmonary and aortic valves between the ventricles and the arteries. During one cardiac cycle a sequence of mechanical events occur, starting when blood in the right atrium is forced into the right ventricle by contraction of the atria. The blood in the right atrium has been collected from all veins in the body, except for the veins from the lungs. When the right ventricle is filled with blood, it contracts and forces the blood into the pulmonary artery and further to the lungs where it is oxygenated. The oxygenated blood passes through the pulmonary veins to the left atrium, which, once it is filled, contracts and forces the blood to the left ventricle. When the left ventricle contracts, the blood flows to all arterial vessels in the body, except for the lungs, into the venous system and back to the right atrium again.

The myocardium, i.e., the wall of the heart, is mainly composed of muscle cells which exercise mechanical force during contraction. The mechanical force of the muscle cells is triggered by electrical impulses; a conduction system of specialized cells in the myocardium spreads the electrical impulse throughout the heart. The cardiac cycle consists of two phases; activation (contraction) and recovery (relaxation) which in electrical terms are referred to as depolarization and repolarization. Depolarization is a rapid change of the membrane potential of the cell. The depolarization spreads to neighboring cells so that the electrical impulse propagates. After depolarization, the cell immediately

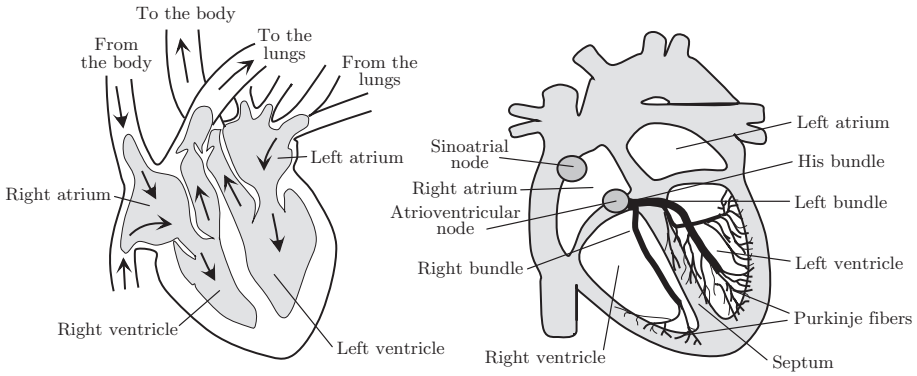

Figure 2.1: Anatomy of the heart. Reprinted with permission from [1].

starts its repolarization to return to its resting state. During this period of time, called refractory period, the cell cannot depolarize.

In the normal heart, the cardiac cycle is initiated by an electrical impulse originating from the sinoatrial node, the natural pacemaker of the heart situated in the right atrium, see Fig. 2.1. The electrical impulse propagates through the right and left atria to the atrioventricular (AV) node, where it is collected and delayed before it continues to the bundle of His, which is the only electric connection between the AV node and the ventricles. The ventricular conduction system consists of the rapidly conducting left and right bundle branches and the Purkinje network. During normal sinus rhythm, the rate of electrical impulses which causes the heart to beat is determined by the autonomic nervous system.

2.2 The Heart during AF

Atrial fibrillation is the most common sustained cardiac arrhythmia in clinical practice. The prevalence of AF increases with age, being 0.4–1% in the general population and 8% for octogenarians [2]. While AF is not generally considered life-threatening, there is a risk of blood clots forming in the atria which leads to increased risk of stroke. The rate of stroke among patients with AF averages 5% per year, which is two to seven times higher than that of the general population [2].

In contrast to normal sinus rhythm, electrical impulses may originate from many different areas in the atria during AF. The exact mechanisms of AF

remain uncertain. The different theories involve two main processes: rapidly depolarizing foci, and reentry circuits [3]. The rapidly depolarizing foci are usually located in the pulmonary veins, but can also occur in the right atria, or (more rarely) in superior vena cava or coronary sinus [4]. The refractory periods of the cells in the conduction system are usually shortened during AF, and, since activation of the cells can occur immediately after the refractory period, this facilitates the forming of electrical reentry loops in the atria.

The irregular atrial activity during AF causes the atria to quiver rather than to contract, which leads to insufficient heart function. Since the atria beats abnormally fast during AF, it is labeled as an atrial tachyarrhythmia.

As a consequence of the rapid atrial rate during AF, the ventricular response is rapid and irregular. However, AV nodal refractoriness prevents the heart from racing. Electrical impulses from the atria are conducted to the ventricles through the AV node, and, if the cells of the AV node are refractory the atrial impulses are blocked. Several complex mechanisms determine the ventricular response during AF; the AV nodal refractory period and the conduction time through the AV node are dependent on intrinsic AV nodal characteristics as well as the timing and strength of the arriving atrial impulses. Concealed conduction, which occurs when an atrial impulse traverse part of the AV node but is not conducted through the ventricles, influences the conduction of subsequent atrial impulses [5]. In addition, the existence of two dominant paths through the AV node, each of them having different electrophysiological properties has been documented [6].

2.3 Diagnosis and Treatment

Atrial fibrillation is generally diagnosed from the surface ECG to confirm its presence. The ECG, which reflects the electrical activity of the heart as measured on the body surface, is an important tool when studying the function of the heart and diagnosing different cardiac diseases. The standard 12-lead ECG is acquired using ten electrodes, of which one is located on each wrist and ankle joint, and the remaining six are located on the chest. When recording the ECG over longer periods of time, it is common to use only three electrodes placed on the chest.

During normal sinus rhythm, each heartbeat in the ECG signal consists of a P wave, a QRS complex, and a T wave [7]. The P wave corresponds to atrial activation, the QRS complex corresponds to activation of the ventricles, and the T wave corresponds to ventricular recovery, see Fig. 2.2. In AF, the P wave is replaced by an undulating baseline, where the waves are referred to as f waves. In atrial flutter, which is another type of atrial tachyarrhythmia,

the P waves are replaced by F waves which are slower and more regular than the f waves during AF. Examples of ECG signals during normal sinus rhythm, AF and atrial flutter are given in Fig. 2.3.

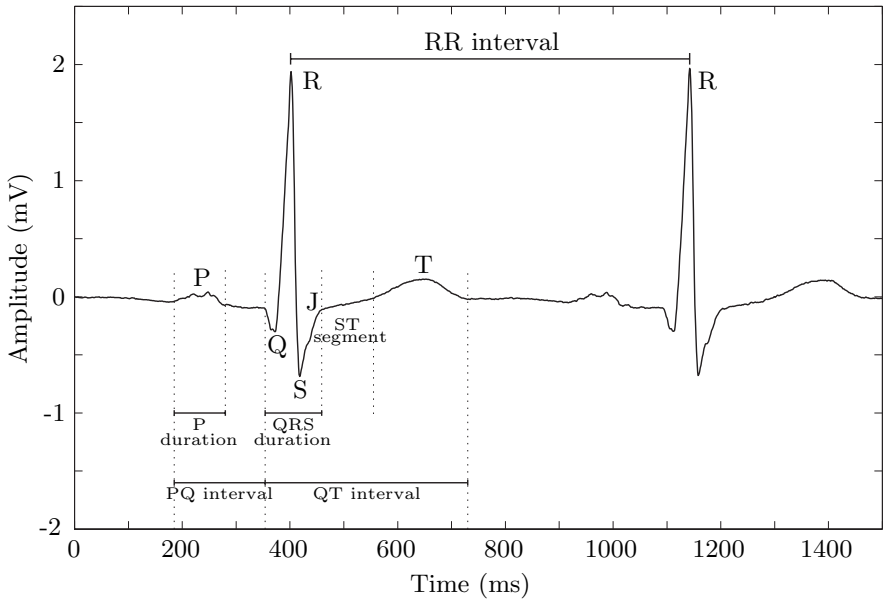

Figure 2.2: Different parts of the ECG signal during normal sinus rhythm. Reprinted with permission from [1].

The medical history of the patient is also considered when diagnosing AF. In some patients transesophageal echocardiography is used in which ultrasound images the anatomy and function of the heart. Intracardiac electrograms are normally only recorded if the patient is undergoing invasive treatment. Atrial fibrillation may be paroxysmal or sustained, the former being occasional episodes of fibrillation interrupting normal sinus rhythm. Sustained AF can be further divided into persistent AF, which may terminate using certain treatment, and permanent AF. In new-onset episodes of AF, i.e. < 48 hours, spontaneous termination is common [8], whereas long-standing persistent AF, e.g. 1 year, usually leads to permanent AF [2]. About 18% of paroxysmal AF evolve to permanent AF over 4 years [9].

Cardioversion denotes restoration of sinus rhythm in patients with persistent AF and can be achieved by means of electrical shock (electrical cardiover-

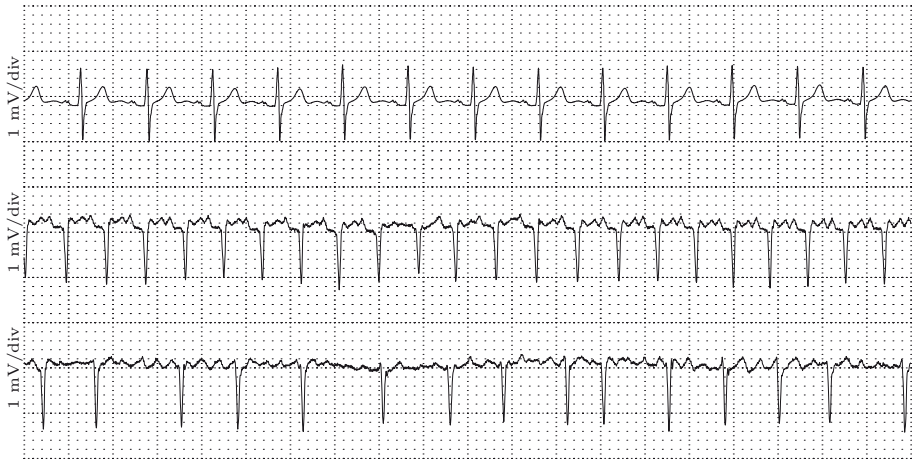

Figure 2.3: Different examples of ECG signals during (top) normal sinus rhythm, (middle) atrial flutter, and (bottom) AF. Reprinted with permission from [1].

sion) or drugs (pharmacological cardioversion). In more than 90% of new-onset AF, electrical cardioversion terminates AF [10]. Electrical shocks are usually delivered noninvasively, but may also be delivered invasively. A wide range of drugs are used for pharmacological cardioversion, with varying efficacies [8]. For new-onset AF, the success rate is about 50% 1.5 hour after drug administration [11]. Pharmacological cardioversion is ineffective for AF of duration longer than 7 days [11]. Recurrence of AF is common after cardioversion, and antiarrhythmic drugs are often needed for maintenance of sinus rhythm. A serious side effect of such drugs is that they may induce other cardiac arrhythmias [12].

In permanent AF, when cardioversion has failed or not been attempted, conventional treatment consists of heart rate control and anticoagulants to prevent clots from forming in the atria [12].

In recent years ablation therapy for treatment of AF has quickly evolved. Today, ablation offers a potential curative strategy for patients with paroxysmal and persistent or permanent AF. Ablation therapy has proved to be superior to currently available antiarrhythmic drugs in the maintenance of sinus rhythm [13]. In catheter ablation, energy is applied for controlled destruction of arrhythmia-generating tissue in the atria. Several different ablation techniques and a variety of energy sources may be used, although RF ablation targeting

the pulmonary veins is the most common procedure. This technique aims at isolating the rapidly depolarizing foci that are usually located in the pulmonary veins. Other AF substrate sites can be identified and targeted during the ablation procedure, guided by the atrial electrograms. In some cases the atria are segmented by creation of linear lesion, to prevent atrial impulses from forming reentry loops [14]. However, it is important to recognize that catheter ablation of AF is a demanding technical procedure that may result in complications. Hence, patients should only undergo AF ablation after carefully considering the risks and benefits of the procedure [14].

Chapter 3

Extraction of Atrial Activity

The ventricular activity in the ECG signal has much larger magnitude than the atrial activity, and thus needs to be suppressed before the atrial activity can be studied. Since the atrial and ventricular activity overlap spectrally, linear time-invariant filtering is unsuitable for this purpose. Instead, atrial activity extraction is usually performed employing average beat subtraction [15–19], or source separation methods [20–25]. While the average beat subtraction methods extract the atrial activity of a specific ECG lead, the source separation methods derive a global atrial signal with contributions from all leads. In this chapter it is assumed that the QRST complexes have been detected and that AF is known to be present in the signal.

3.1 Average Beat Subtraction Methods

During AF, the atrial activity is decoupled from the ventricular activity. Hence, atrial activity that coincide with QRST complexes may be removed by averaging beats. Prior to average beat subtraction, the detected QRST complexes should be classified according to their morphology. Similarity of QRST complexes is usually quantified by correlation, such that if the correlation exceeds a certain threshold, the QRST complexes are considered to belong to the same class of QRST morphology. In the next step, template QRST complexes are obtained by averaging the QRST complexes in each morphology class. Finally, the template QRST complex can be subtracted from the individual QRST complexes in the corresponding morphology class, where it is important that the

template is correctly aligned in time.

The technique for obtaining atrial activity from the ECG by subtracting an average QRST complex was first presented in [15]. Since then several improvements, such as spatiotemporal QRST cancellation [16], have been proposed. In this approach, the QRST complexes are spatially aligned by shifting signal energy between the different leads. In detail, the atrial activity is assumed to be uncorrelated to the ventricular activity during AF. Hence, each beat $\mathbf{Y}$, consisting of N samples from L leads, can be modeled as a sum of ventricular activity $\mathbf{Y}_V$, atrial activity $\mathbf{Y}_A$, and noise $\mathbf{W}$,

$$\mathbf{Y} = \mathbf{Y_V} + \mathbf{Y_A} + \mathbf{W}. \tag{3.1}$$

The ventricular activity in $\mathbf{Y}$ is modeled as

$$\hat{\mathbf{Y}}_\mathbf{V} = \mathbf{J}(\tau)\bar{\mathbf{X}}\mathbf{S}, \tag{3.2}$$

where $\mathbf{J}(\tau)$ is a time shift matrix, $\bar{\mathbf{X}}$ is the average QRST complex of the corresponding morphology class, and $\mathbf{S}$ is a spatial alignment matrix. The time shift matrix $\mathbf{J}(\tau)$ corrects for misalignment in time between $\mathbf{Y}_V$ and $\bar{\mathbf{X}}$, while the spatial alignment matrix $\mathbf{S}$ compensates for alterations of the electrical axis. $\mathbf{S}$ is composed of a diagonal scaling matrix, $\mathbf{D}$, and a rotation matrix, $\mathbf{Q}$, such that

$$\hat{\mathbf{Y}}_\mathbf{V} = \mathbf{J}(\tau)\bar{\mathbf{X}}\mathbf{D}\mathbf{Q}, \tag{3.3}$$

The aim is to estimate the matrices $\mathbf{Q}$, $\mathbf{D}$, and the time-shift τ of $\mathbf{J}(\tau)$, such that

$$\mathbf{Y} - \hat{\mathbf{Y}}_\mathbf{V} = \mathbf{W} + \mathbf{Y}_A. \tag{3.4}$$

Hence, not only the noise but also the atrial activity will limit how well $\hat{\mathbf{Y}}_\mathbf{V}$ fits $\mathbf{Y}$. In order to improve the cancellation performance, an estimate of the atrial activity $\tilde{\mathbf{Y}}_A$ is subtracted from the signal prior to QRST cancellation, defining

$$\mathbf{Z} = \mathbf{Y} - \tilde{\mathbf{Y}}_A. \tag{3.5}$$

This procedure is referred to as AF reduction, and leads to the following minimization problem

$$\epsilon^2_{min} = \min_{\mathbf{D},\mathbf{Q},\tau} ||\mathbf{Z} - \mathbf{J}(\tau)\bar{\mathbf{X}}\mathbf{D}\mathbf{Q}||^2_F, \tag{3.6}$$

where $||\mathbf{A}||^2_F$ denotes the Frobenius norm, defined by $\mathrm{tr}\{\mathbf{A}\mathbf{A}^T\}$.

Since $\mathbf{Q}$ and $\mathbf{D}$ cannot be maximized independently, and a closed-form solution is difficult to find, the minimization problem is solved using an alternating iterative approach. Minimization with respect to the time-lag, τ, is done by a

grid-search in the interval $[-\Delta, \Delta]$. The optimal $\mathbf{Q}$ and $\mathbf{D}$ are determined for each value of τ, and the $\mathbf{Q}$, $\mathbf{D}$, and $\mathbf{J}(\tau)$ corresponding to the smallest error are chosen. Finally, the spatially and temporally aligned average beat is subtracted from each beat of the ECG, producing a residual signal, see Fig. 3.1.

An extension to the spatiotemporal QRST cancellation technique was proposed by Lemay et al. [18], where separate QRS and T wave templates were considered. The rationale for using separate templates is that the physiological origin of the QRS and T waves differ, and hence, the morphology of the T wave may be different even if the QRS complex is similar and vice versa.

A limitation of the average beat subtraction methods is that a sufficiently large number of QRST complexes with similar morphology are required to create an average beat. Hence, methods based on average beat subtraction cannot be used to extract ventricular activity from short segments of ECG. Another problem with these methods is that incompletely cancelled QRST complexes introduce spiked artifacts in the residual ECG, which complicates the analysis of the extracted atrial activity.

3.2 Principal Component Analysis

In principal component analysis (PCA), an $N \times M$ data matrix $\mathbf{X}$ consisting of M mutually correlated signals of length N, is transformed into an $N \times M$ matrix $\mathbf{Y}$ consisting of M uncorrelated principal components of length N, by applying an orthonormal linear transform, defined by the $N \times N$ matrix $\mathbf{P}$ [26],

$$\mathbf{Y} = \mathbf{P}^T \mathbf{X}. \tag{3.7}$$

The derivation of $\mathbf{P}$ is based on the assumption that each signal $\mathbf{x}_m$, $m = 1, \ldots, M$, represents a zero-mean random process, characterized by the correlation matrix $\mathbf{C}_x$. The principal components $\mathbf{y}_m$, i.e. the columns of $\mathbf{Y}$, are ordered according to variance, such that the first principal component $\mathbf{y}_1$ has the largest variance. Hence, the first column $\mathbf{p}_1$ of the transformation matrix $\mathbf{P}$ is chosen to maximize

$$E\{\mathbf{y}_1^T \mathbf{y}_1\} = E\{(\mathbf{p}_1^T \mathbf{x}\mathbf{x}^T \mathbf{p}_1\} = \mathbf{p}_1^T E\{\mathbf{x}\mathbf{x}^T\}\mathbf{p}_1 = \mathbf{p}_1^T \mathbf{C}_x \mathbf{p}_1, \tag{3.8}$$

where $\mathbf{p}_1$ is subjected to the constraint $||\mathbf{p}_1|| = 1$. The optimal solution to maximization of (3.8) under this constraint is given by $\mathbf{p}_1 = \mathbf{e}_1$, i.e, the normalized eigenvector corresponding to the largest eigenvalue of the correlation matrix $\mathbf{C}_x$. Hence, the first principal component $\mathbf{y}_1$ is given by $\mathbf{e}_1^T \mathbf{x}$. The following principal components are chosen under the additional constraint that they should be orthogonal to the previous principal components, such that

$$E\{\mathbf{y}_m^T \mathbf{y}_k\} = E\{\mathbf{p}_m^T \mathbf{x}\mathbf{x}^T \mathbf{p}_k\} = \mathbf{p}_m^T \mathbf{C}_x \mathbf{p}_k = 0, \quad m \neq k. \tag{3.9}$$

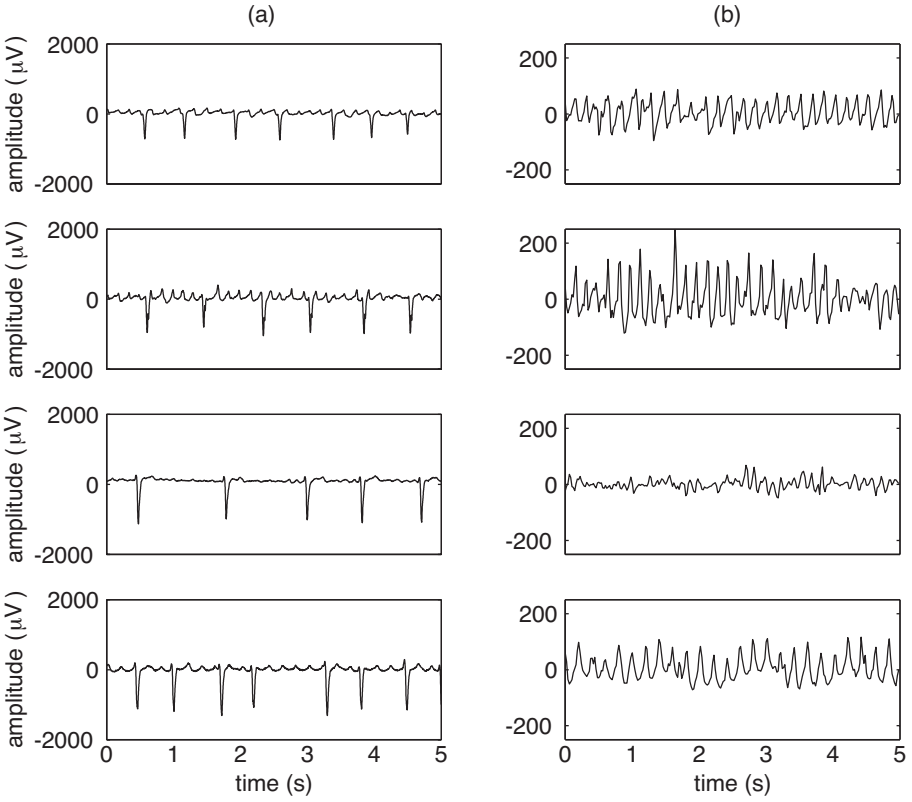

Figure 3.1: (a) Examples of ECG signals from patients with AF and (b) the corresponding residual ECG obtained using spatiotemporal QRST cancellation [16]. Note that the scaling of the residual ECG is magnified.

The solution is given by $\mathbf{p}_k = \mathbf{e}_k$. Hence, using PCA, the rows of $\mathbf{P}$ are given by the eigenvectors of $\mathbf{C}_x$.

The principal components can also be obtained directly from the data matrix $\mathbf{X}$ using singular value decomposition (SVD) [26]. The SVD theorem states that an $M \times N$ matrix $\mathbf{X}$ can be decomposed as

$$\mathbf{X} = \mathbf{U}\mathbf{\Sigma}\mathbf{V}^T, \tag{3.10}$$

where $\mathbf{U}$ is an orthonormal $N \times N$ matrix with left singular columns, $\mathbf{V}$ is an orthonormal $M \times M$ matrix with right singular columns, and $\mathbf{\Sigma}$ is a diagonal $N \times M$ matrix containing the singular values. The eigenvectors associated with PCA are obtained as the left singular vectors of $\mathbf{U}$, i.e. $\mathbf{U} = \mathbf{P}$.

Assuming that atrial and ventricular activity are uncorrelated during AF, PCA can be used to extract atrial activity from the ECG. In the work by Raine et al. [20], PCA was employed to extract the atrial activity from 20-s 12-lead ECGs; the resulting principal component with the largest contribution from lead V1, which is generally the lead with the most prominent f waves, was selected to represent atrial activity. This blind source separation approach is closely related to the independent component analysis techniques presented in Sec. 3.3. However, in PCA independence between sources are measured entirely by means of correlation; the higher order moments are disregarded.

Principal component analysis can also be applied to separate atrial and ventricular activity in consecutive QRST segments from one lead [17]. In that study, the first principal component was assumed to consist of ventricular activity, since the magnitude, and hence, the variance of the signal is larger in ventricular activity than in atrial activity. The principal components corresponding to the smallest eigenvalues were assumed to be noise. The atrial activity of the m:th segment $\hat{\mathbf{x}}_m$ was reconstructed from the remaining principal components $\mathbf{y}_i, \quad i = k_1, \ldots, k_n$, which were assumed to consist of atrial activity, using the inverse transform

$$\hat{\mathbf{x}}_\mathbf{m}(n) = \sum_{i=k_1}^{k_n} \mathbf{P}^{-1}_{m,i}\mathbf{y}_i(n). \tag{3.11}$$

The segments of atrial activity were then put together to create a continuous signal with atrial activity; bandpass filtering was applied to avoid undesired edge effects. A general problem with the blind source separation approach is to select sources corresponding to atrial activity, i.e, the choice of k_1 and k_n; no criteria for this selection was given in this work.

In another study [19], the extracted principal component corresponding to ventricular activity was used as a template QRST complex, and subtracted

from each QRST complex to obtain the atrial activity. In order to account for differences in amplitude, scaling was applied to the template QRST complex before subtraction. Care was taken to avoid sudden transitions at the beginning and end of the subtracted template. Although the template QRST complex is obtained using PCA rather than averaging, the technique is essentially similar to that used in average beat subtraction methods. Differences in QRST morphology are not considered in this method; all QRST complexes occurring within a certain time frame are used to generate the template QRST complex.

A method for cancellation of ventricular activity based on one single beat was presented in [18], in which a template TU wave was created using PCA based on the JQ intervals of all available leads, and the atrial activity of the QRS segment was interpolated from adjacent JQ segments. Since T wave morphology has proved to be quite similar in different leads, a dominant T wave $T_{dom}(t)$ may be obtained from SVD of the matrix $\mathbf{X}$ containing the N samples during the JQ interval of the L leads. The first principal component corresponds to $T_{dom}(t)$. The T wave of each lead is assumed to be sufficiently modeled using $T_{dom}(t)$ and its derivatives. In order to eliminate noise in $T_{dom}(t)$, which may influence the derivatives considerably, $T_{dom}(t)$ is approximated by a smooth function

$$f(t) = p_1 \left(p_2 + \frac{1}{1 + e^{p_3(t-p_5)}} \frac{1}{1 + e^{p_4(t-p_5)}} \right), \tag{3.12}$$

where p_1 is a scale factor, p_2 sets the initial value, p_3 and p_4 are parameters for the positive and negative slope, and p_5 is the timing of the T wave apex. A function which accounts for the unlikely presence of a U wave is incorporated in the $T_{dom}(t)$ template. The U wave is approximated by a gaussian function

$$g(t) = p_6 e^{-\left(\frac{t-p_6}{p_7}\right)}, \tag{3.13}$$

where p_6 is an overall scaling factor, p_7 is the width and p_8 is the timing of the U wave apex. The parameters p_i, $i = 1, \ldots, 8$ were found by fitting $f(t) + g(t)$ to $T_{dom}(t)$. A linear combination of $f(t)$, $f'(t)$, $f''(t)$ and $g(t)$ was fitted to the JQ segment of each lead, and atrial activity was estimated by subtracting the acquired template TU wave. The atrial activity of the QRS segment of each lead was modeled as a finite sum of sinusoids

$$s(t) = \sum_{k=1}^{P} \alpha_k \cos(2\pi f_k t) + \beta_k \sin(2\pi f_k t), \tag{3.14}$$

where the frequencies f_k was uniformly distributed between 0-10 Hz. The coefficients α_k and β_k were determined from preceding and subsequent JQ

intervals using least squares estimation, and the atrial activity of the QRS segment was interpolated using these coefficients. Finally, the atrial signal was obtained by merging the interpolated sinusoids of the QRS segment with surrounding JQ intervals.

A criticism towards this method is that atrial activity of the QRS segment is estimated entirely based on the atrial activity in adjacent JQ segments. Therefore, this method is only intended for QRST cancellation in short segments of ECG, when the number of QRST complexes in each cluster is insufficient for average beat subtraction methods.

3.3 Independent Component Analysis

When applying blind source separation methods to the ECG signals, each lead of the ECG is assumed to consist of a linear combination of sources with atrial and ventricular origins and noise. The sources are considered independent since the atrial and the ventricular activity are decoupled during AF. Mathematically, the M observed ECG signals $\mathbf{x}(t) = [x_1(t), x_2(t), \ldots, x_M(t)]^T$, are given by

$$\mathbf{x}(t) = \mathbf{A}\mathbf{s}(t), \tag{3.15}$$

where $\mathbf{s}(t) = [s_1(t), s_2(t), \ldots, s_M(t)]^T$ are the M unknown independent sources, and $\mathbf{A}$ is an unknown mixing matrix. Hence, the sources can be estimated from the observed signals using

$$\hat{\mathbf{s}}(t) = \mathbf{W}\mathbf{x}(t). \tag{3.16}$$

Solving the blind source separation problem is therefore a matter of estimating the coefficients of $\mathbf{W}$. This is done by maximizing the independence between the estimated sources $\hat{\mathbf{s}} = [\hat{s}_1(t), \hat{s}_2(t), \ldots, \hat{s}_M(t)]^T$.

In independent component analysis (ICA), the independence of the sources is maximized based on higher order statistics or entropy measures [27]. The signals are assumed to have zero mean, which can easily be fixed by subtracting the mean value, and to be white, i.e. uncorrelated with unit variance. Since PCA whitens the signal, it is often a preprocessing step in ICA algorithms. The sources are required to be nongaussian. Maximizing independence of the sources can be done by minimizing gaussianity of the sources, since sums of nongaussian variables are closer to gaussian than the original signal according to the central limit theorem. Gaussianity of a signal $\mathbf{y}$ can be measured using entropy, defined by

$$H(\mathbf{y}) = -\int p_{\mathbf{y}}(\boldsymbol{\eta}) \log p_{\mathbf{y}}(\boldsymbol{\eta}) d\boldsymbol{\eta}, \tag{3.17}$$

where $p_{\mathbf{y}}(\boldsymbol{\eta})$ denotes the probability of $\mathbf{y} = \boldsymbol{\eta}$. The entropy is largest if $\mathbf{y}$ has a gaussian distribution.

The Fast ICA algorithm for estimating several independent components [27], using an iterative scheme to obtain the independent sources, has been employed to separate atrial activity from ventricular activity in the ECG signal [21]. Figure. 3.2 displays a 12-lead ECG from a patient with AF and the corresponding decomposed sources using ICA. Recently, a robust ICA method for which no prewhitening is required, and which can be used to decompose real as well as complex signals was presented [25]; this ICA method was applied to ECG signals with AF in the frequency domain, and the extracted sources were transformed back to time domain.

Once the independent sources have been separated, each source needs to be identified as ventricular activity, atrial activity or noise. There is no unanimous criteria for identifying sources with atrial activity; measures based on the sample distribution as well as on the spectral content of the sources have been proposed for this task.

The sample distributions of the different sources can be classified according to their gaussianity, which can be quantified using kurtosis,

$$\mathcal{K}(y) = E\{y^4\} - 3(E\{y^2\})^2. \tag{3.18}$$

Kurtosis is zero for gaussian random variables, while subgaussian variables, e.g., the uniform distribution, have negative kurtosis and supergaussian variables, e.g., the laplacian distribution, have positive kurtosis. The ventricular activity is more spiky, and has hence larger values of $\mathcal{K}$ than does noise and atrial activity. Sources with $\mathcal{K} < 0$ and spectral content between 3–12 Hz were identified as atrial activity in the work by Rieta et al. [21], whereas identification of atrial activity was based solely on spectral content in the work by Zarzozo et al. [25].

Castells et al. [22] introduced a second step following ICA separation, second order blind identification, which aims at separating atrial activity from noise. First, the separated sources from ICA containing ventricular activity were removed; these sources were identified based on their high kurtosis $\mathcal{K} > 1.50$. The remaining sources, which were considered to contain atrial activity and noise, were separated based on spectral content by minimizing correlation at different time lags. In this approach, the independent sources $\mathbf{s}$ obtained from ICA are assumed to be an orthogonal transformation of the real sources $\mathbf{z}$ containing atrial activity and noise, so that

$$\mathbf{s} = \mathbf{Q}\mathbf{z} \tag{3.19}$$

where $\mathbf{Q}$ is a Givens rotation matrix. Since the sources should be uncorrelated

Figure 3.2: Illustrations of ICA for (a) a 12-lead ECG from a patient in AF. (b) The separated sources are reordered from lower to higher kurtosis value. The atrial activity is contained in source #1. Reprinted from [21] with permission.

for all time-lags τ_i, the correlation matrices

$$\mathbf{C}(\tau_i) = E[\mathbf{z}(t)\mathbf{z}^T(t-\tau_i)] \tag{3.20}$$

should be diagonal. The optimal $\mathbf{Q}$ is the one that maximizes the joint diagonalization of $\mathbf{C}$ for each τ_i simultaneously, so that

$$\hat{\mathbf{Q}} = \arg\max_{\mathbf{V}} J(\mathbf{V}), \tag{3.21}$$

where

$$J(\mathbf{V}) = \sum_{i=1}^{N} ||\text{diag}[\mathbf{V}^T\mathbf{C}(\tau_i)\mathbf{V}]||^2. \tag{3.22}$$

The correlation matrices were computed for $\tau_i = [0, 20, 40, \ldots, 320]$ ms, i.e. corresponding to a maximum of approximately two f waves, since significant correlation can be expected at these lags. Following second order blind identification, only one of the sources had a spectral peak in the 3–10 Hz region; this source was considered to contain the atrial activity.

Another approach to include temporal information when separating sources was proposed by Vayá et al. [23]. In this work, a convolutive linear mixing model, where the mixing matrix A was assumed to consist of FIR filters rather than constants, was considered. The performance of the Infomax algorithm, which assumes a convolutive linear mixing of sources, was compared to that of the Fast ICA algorithm, which assumes instantaneous mixing of sources, showing that the Fast ICA was better suited for atrial activity extraction. Hence, it was concluded that the instantaneous linear mixing model was sufficient for atrial and ventricular activity in the ECG.

A semi-blind source extraction technique, in which the source that best agrees with a given set of AR parameters is extracted, was used to extract atrial activity from the ECG in [24]. First, atrial activity was roughly estimated from non-QRST intervals of lead V1, which is assumed to have the largest atrial activity, and an initial set of AR parameters were obtained from this crude atrial activity estimate. The source best agreeing with these AR parameters was extracted, and a new set of AR parameters were obtained from the extracted atrial activity. This iterative procedure continued until the AR parameters had converged. Using this approach, the problem of how to determine which sources that contain atrial activity is essentially avoided. However, as sufficiently long non-QRST intervals are required to estimate the initial set of AR parameters, the use of this method is restricted to ECGs with slow ventricular rate.

3.4 Performance Evaluation

Since the true atrial activity is not known in ECG signals, it is difficult to evaluate atrial activity extraction performance. However, some measures that quantifies performance based on time domain or frequency domain characteristics of the extracted atrial activity have been proposed. The amplitude of the extracted atrial activity in QRST intervals was compared to that of non-QRST intervals [28]; if the amplitude in a QRST segment was above a certain data dependent threshold, the residual was considered to be significant [18]. In addition to the amplitude, the energy in QRST segment may also be considered [19]. Since the criteria are based solely on minimizing residuals, blanking of QRST segments would produce an excellent result according to these measures. Spectral concentration, defined as the ratio between spectral power in a small interval centered around the dominant spectral peak and the total spectral power, has been used to evaluate atrial activity extraction performance [22, 23]; a high spectral concentration is assumed to correspond to better atrial activity extraction, since large QRST residuals would cause the spectrum to become less distinct. This measure generally favors source separation techniques, since the sources with atrial activity are often selected based on frequency content in these methods.

Simulated signals may be used to overcome the problem with unknown atrial activity. Artificial AF signals may be generated using simulated atrial activity combined with real ECG signals from patients in normal sinus rhythm, where the P waves have been removed. Several methods for generating artificial atrial activity have been proposed. In [22], atrial activity signals was generated from the TQ intervals of patients in AF. The atrial activity in QRST segments was generated by extrapolation of adjacent TQ segments; the f waves in preceding TQ segment were replicated within the QRST interval, but linearly weighted so that the weights were one in the beginning of the QRST segment and zero in the end, similarly the f waves of subsequent TQ interval was replicated and weighted by zero in the beginning of the segment but one in the end.

In [16], simulated atrial activity signals were modeled by sawtooth signals, generated using a linear combination of a sinusoid and its $M-1$ harmonics,

$$s(n) = -\sum_{m=1}^{M+1} a_m(n) \sin(m2\pi f_0 n + \frac{\Delta f}{f_f} \sin(2\pi f_f n)), \tag{3.23}$$

where the fundamental f_0 has a maximum frequency deviation of Δf and the modulation frequency f_f. The time-varying amplitudes of the fundamental and the harmonics, denoted $a_1(n)$ and $a_m(n), m = 2, \ldots, M+1$, respectively, are

given by

$$a_m(n) = \frac{2}{m\pi}(a_m + \Delta a_m \sin(2\pi f_a n)), \tag{3.24}$$

where Δa_m is the modulation peak amplitude and f_a is the modulation frequency.

In [18], a more advanced model which makes use of electroanatomical information on the atria as well as volume conduction theory, was used to simulate atrial activity. In this approach, a 3-D model of the human atria was constructed from magnetic resonance images [29]. The properties of the atrial conduction cells were modeled using a detailed ionic model. Atrial fibrillation was induced in the model by rapid pacing in the left atrium; the properties of the atrial conduction cells had been modified to create substrates for AF. Simulated signals modeling the atrial activity of ECGs were computed using a complementary torso model, also this constructed from MR images.

When the atrial activity is known, as is the case with simulated signals, the atrial activity extraction performance can be quantified as mean square error or using cross correlation between true and extracted atrial activity.

Chapter 4

Characterization of Atrial Activity

The atrial activity of the ECG exhibit both intra- and interpatient variability with respect to amplitude, morphology, repetition rate and regularity of the f waves.

Different methods to extract features charactering f waves have been proposed, including time-frequency analysis [30–32], morphology analysis [31, 33], complexity analysis [34, 35], and spatial analysis [36–38]. In this chapter we assume that the atrial activity of the ECG has been extracted, cf. Ch 3; the extracted atrial activity is here referred to as residual ECG.

4.1 Time-Frequency Analysis

The AF frequency, i.e. the repetition rate of the f waves, is an important characteristic of the atrial activity in the ECG. It can be estimated from the maximum peak of the power spectrum of the residual ECG. By comparing endocardially recorded electrograms to ECG signals, it has been shown that AF frequency can be used as an index of the average intra-atrial fibrillatory cycle length [39–41].

The AF frequency can be used for monitoring of drug effects [42], as well as for predicting spontaneous or drug-induced AF termination; a low AF frequency has proved to be a predictor of spontaneous AF termination [35, 43]. When the AF frequency is below 6 Hz the likelihood of successful pharmaceutical cardioversion is higher [40, 44]. The risk of early AF recurrence is also higher for patients with higher AF frequency [45].

The atrial refractory period, and hence the AF frequency, is known to be affected by autonomic modulation [46]. Hence, AF frequency has been used to monitor circadian variations as well as the effects of parasympathetic and sympathetic stimulation. Studies show that the AF frequency decreases during night and increases in the morning [47–49], and that carotide sinus massage (parasympathetic stimulation) [50], head-up tilt (sympathetic stimulation) [51], and controlled respiration [52] alters AF frequency.

4.1.1 Short-time Fourier Transform

In order to explore the time-varying properties of AF, time-frequency analysis has been suggested. The basic approach to time-frequency analysis is to segment the signal and calculate the Fourier spectrum for each segment. The short-time Fourier transform is defined by

$$W_{STFT}(n,k) = \sum_{m=-K/2+1}^{K/2} s(n+m)w(m)e^{-j2\pi km}, \tag{4.1}$$

where $s(n)$ is the signal, $w(n)$ is a window function, and K is the window length and the number of frequency samples. The segments may be overlapping. A larger value of K gives better frequency resolution, but poorer resolution in time. Hence, the choice of segment size is a trade-off between time and frequency resolution.

4.1.2 Other Time-Frequency Distributions

While the STFT depends linearly on the signal, there are other time-frequency distributions that depend quadratically on the signal, e.g. the Wigner–Ville distribution (WVD), defined by

$$W_{WVD}(n,k) = \sum_{m=-L}^{L} \sum_{l=-L}^{L} A_z(m,l)e^{-j2\pi ln/N}e^{-j2\pi km/N}, \tag{4.2}$$

where the ambiguity function $A_z(m,l)$ is given by

$$A_z(m,l) = \sum_{p=-L}^{L} z(p+m)z^*(p-m)e^{j2\pi lp/N}. \tag{4.3}$$

The signal $z(n)$ is the analytic equivalent of the signal $s(n)$,

$$z(n) = s(n) + j\mathcal{H}(s(n)) \tag{4.4}$$

where $\mathcal{H}(s(n))$ is the Hilbert transform of $s(n)$. The advantage of these quadratically dependent distributions is the improved time-frequency resolution. However, quadratic distributions of multicomponent signals introduce cross-terms between components.

There are other quadratic distribution, e.g. the Choi–Williams distribution (CWD), which is similar to the WVD except for that certain regions of the ambiguity plane are weighted down using a kernel function, $f(m,l)$, so that

$$W_{CWD}(n,k) = \sum_{m=-L}^{L} \sum_{l=-L}^{L} f(m,l) A_z(m,l) e^{-j2\pi ln/N} e^{-j2\pi km/N}. \tag{4.5}$$

In the CWD the kernel, defined by

$$f(m,l) = e^{-\frac{m^2 l^2}{\sigma}}, \tag{4.6}$$

weights down cross-terms between frequency components that do not occur at the same time or at the same frequency. In [53] a new set of kernel functions were presented. One of the kernels, defined by

$$f(m,l) = \frac{8J_2(\alpha ml)}{(\alpha ml)^2}, \tag{4.7}$$

where $J_2(\cdot)$ is the Bessel function of first kind order 2, was proposed for time-frequency analysis of atrial activity from the ECG; the parameter α was set to 0.5 for this application.

4.1.3 Cross Wigner–Ville Distribution

Despite the efforts made to improve atrial activity extraction, the residual ECG often contains noise such as muscular artifacts and remainders of cancelled QRST complexes, that can cause analysis to become inaccurate. In [30], a method based on the cross Wigner–Ville distribution (XWVD) was proposed for robust estimation of the AF frequency trend in the presence of noise. The XWVD is defined by

$$W_{XWVD}(n,k) = \sum_{m=-L}^{L} \sum_{l=-L}^{L} A_{z_1,z_2}(m,l) e^{-j2\pi ln/N} e^{-j2\pi km/N}, \tag{4.8}$$

where

$$A_{z_1,z_2}(m,l) = \sum_{p=-L}^{L} z_1(p+m) z_2^*(p-m) e^{j2\pi lp/N} \tag{4.9}$$

and $z_1(n)$ and $z_2(n)$ are two analytical signals. The XWVD may be used to extract the local frequency of a time-varying, repetitive signal.

Instantaneous frequency estimation of can be preformed using the XWVD with an iterative procedure. First, a preliminary frequency trend, $\hat{F}_0(n)$ is determined using, e.g., the STFT or the WVD. Then

1. A frequency-modulated sinusoid is reconstructed from the frequency trend.
$$z_{\hat{F}_l}(n) = e^{j2\pi \sum_{i=0}^{n} \hat{F}_l(i)} \tag{4.10}$$

2. The XWVD between $z_{\hat{F}_l}(n)$ and $z(n)$ is computed by
$$W_{XWVD_{l+1}}(n,k) = \sum_{m=-L}^{L} \sum_{l=-L}^{L} z(p+m) z^*_{\hat{F}_l}(p-m) e^{-j4\pi mk/K} \tag{4.11}$$
Peak detection in the XWVD domain results in a new frequency trend, $\hat{F}_{l+1}(n)$.

3. The procedure is repeated until the frequency trend converges
$$\hat{F}_{l+1}(n) - \hat{F}_l(n) = 0 \quad \forall\, n \tag{4.12}$$

The cross-term between the original signal and the reconstructed sinusoid will be large, and hence selected when reconstructing a new sinusoid. In this way, the reconstructed sinusoid converges to the frequency trend of the original signal. A disadvantage of the XWVD approach is that only the fundamental of AF is being used, while the harmonic pattern is not considered when estimating the AF frequency.

4.1.4 Phase-Rectified Signal Averaging

Another approach to robust estimation of the AF frequency in the presence of QRST residuals and noise is by phase-rectified signal averaging (PRSA) [32]. In this approach, the AF frequency is estimated from a signal average $\tilde{x}(k)$, rather than from the original signal $x(n)$. The signal average $\tilde{x}(k)$ is created to enhance quasi-periodic components of the original signal $x(n)$; this is achieved by averaging segments of $x(n)$ centered around certain anchor points n_ν which are selected based on their instantaneous phase.

In [32], n_ν were chosen so that all samples for which the signal is incremented $x(n) > x(n-1)$ were selected as anchor points $x(n_\nu)$. In this way, M different

segments of length $2L+1$ centered around $x(n_\nu)$, $\nu = 1, \ldots, M$, were created. These segments were averaged to produce the phase-rectified signal average,

$$\tilde{x}(k) = \frac{1}{M} \sum_{\nu=1}^{M} x(n_\nu + k), \quad k = -L, \ldots, L-1. \tag{4.13}$$

The AF frequency was estimated by the maximum peak of the power spectrum of $\tilde{x}(k)$ obtained from 5 min of residual ECG during AF. The parameter L influences the properties of $\tilde{x}(k)$; if L is small the effect of averaging is larger but the resulting signal shorter. As frequency resolution increases with segment length, the choice of L is a tradeoff between averaging effect and frequency resolution; $L = 512$ was used in [32], which corresponded to a length of $\tilde{x}(k)$ of approximately 2 s.

The performance of AF frequency estimation using PRSA was compared to that of AF frequency estimation using averaged short-time Fourier spectra, obtained using 50% overlap and a Hamming window of length 1025. Results show that the methods perform equally well for AF frequency estimation from the residual ECG. When attempting to estimate the AF frequency from the original ECG, i.e., in the presence of QRST complexes, the PRSA technique resulted in more accurate estimates, although the QRST cancellation had greater influence on performance than did PRSA. It was concluded that PRSA improves AF frequency estimation in very noisy conditions. A drawback of this approach is the poor time resolution, as only one frequency estimate is obtained for each 5 min segment.

4.2 Morphology Analysis

The harmonic pattern of the residual ECG spectra can be exploited to quantify f wave morphology. The magnitude [31] as well as the phase [33] of the harmonics can be used to monitor morphological changes of the f waves. The exponential decay of the harmonic magnitudes can be used to predict spontaneous termination of AF [35, 54] and AF recurrence following electrical cardioversion [55] as well as to monitor drug induced changes of f wave morphology [42].

4.2.1 The Spectral Template Method

The spectral template method, which makes use of the harmonic pattern of AF was proposed for robust AF frequency trend estimation [31]. The ECG signal is divided into overlapping segments, for which the spectrum, $\mathbf{q}_l$, is obtained using a nonuniform Fourier transform,

$$\mathbf{q}_l = \mathbf{F}\mathbf{W}\mathbf{x}_l, \tag{4.14}$$

where the elements of the $N \times N$ diagonal matrix $\mathbf{W}$ defines a window function. The $K \times N$ matrix $\mathbf{F}$ defines the K-point discrete, nonuniform Fourier transform

$$\mathbf{F} = \begin{bmatrix} \mathbf{1} & e^{-j2\pi\mathbf{f}} & e^{-j2\pi\mathbf{f}2} & \cdots & e^{-j2\pi\mathbf{f}(N-1)} \end{bmatrix}, \tag{4.15}$$

where $\mathbf{f} = [f_0 \cdots f_{K-1}]^T$ is a logarithmically scaled frequency vector, given by

$$f_k = f_0 \cdot 10^{\frac{k}{K}}, \quad k = 0, \ldots, K-1. \tag{4.16}$$

Each observed spectrum $\mathbf{q}_l$ can be modeled by $\tilde{\mathbf{q}}_l$ being a frequency-shifted, ν_l, and amplitude-scaled, a_l, version of a known real-valued spectral template, $\boldsymbol{\phi}_l$,

$$\tilde{\mathbf{q}}_l = a_l \, \mathbf{J}(\nu_l) \, \boldsymbol{\phi}_l, \tag{4.17}$$

where the matrix $\mathbf{J}(\nu_l)$ performs the frequency shift by selecting the appropriate interval of $\boldsymbol{\phi}_l$. The amplitude parameter a_l and the frequency-shift parameter ν_l can be estimated by minimizing the quadratic cost function, $J(\nu_l, a_l)$, such that the model, $\tilde{\mathbf{q}}_l$, optimally matches the true spectrum, $\mathbf{q}_l$,

$$J(\nu_l, a_l) = (\mathbf{q}_l - \tilde{\mathbf{q}}_l)^T \, \mathbf{D} \, (\mathbf{q}_l - \tilde{\mathbf{q}}_l) \tag{4.18}$$

$$= (\mathbf{q}_l - a_l \mathbf{J}(\nu_l)\boldsymbol{\phi}_l)^T \, \mathbf{D} \, (\mathbf{q}_l - a_l \mathbf{J}(\nu_l)\boldsymbol{\phi}_l), \tag{4.19}$$

where $\mathbf{D}$ is a $K \times K$ diagonal matrix designed to weight the error of the frequency components differently, to compensate for the logarithmic frequency scaling. Minimization of (4.19) results in estimates of the frequency-shift $\hat{\nu}_l$ and the amplitude a_l,

$$\hat{\nu}_l = \arg\max_{\nu_l} \left[\mathbf{q}_l^T \mathbf{D}^{\frac{1}{2}} \mathbf{J}(\nu_l) \mathbf{D}^{\frac{1}{2}} \boldsymbol{\phi}_l \right] \tag{4.20}$$

$$\hat{a}_l = \mathbf{q}_l^T \mathbf{D}^{\frac{1}{2}} \mathbf{J}(\hat{\nu}_l) \mathbf{D}^{\frac{1}{2}} \boldsymbol{\phi}_l. \tag{4.21}$$

With the estimates of a_l and ν_l, a model of the observed spectrum is obtained,

$$\hat{\mathbf{q}}_l = \hat{a}_l \, \mathbf{J}(\hat{\nu}_l) \, \phi_l. \tag{4.22}$$

The spectral template is gradually updated to fit the shape of the true spectrum. For the first segment, the spectral template, $\boldsymbol{\phi}_0$, is initiated by

$$\boldsymbol{\phi}_0 = \begin{bmatrix} 0.01 & \cdots & 0.01 & 1 & 0.01 & \cdots & 0.01 \end{bmatrix}^T, \tag{4.23}$$

where $\boldsymbol{\phi}_0$ is 1 at a predefined peak position and 0.01 at all other positions. The spectral template, $\boldsymbol{\phi}_l$, is then updated for each segment through exponential averaging,

$$\hat{\boldsymbol{\phi}}_{l+1} = (1 - \alpha_l)\hat{\boldsymbol{\phi}}_l + \alpha_l \frac{\mathbf{J}(\hat{\nu}_l)\hat{\mathbf{q}}_l}{\|\mathbf{J}(\hat{\nu}_l)\hat{\mathbf{q}}_l\|}, \quad l > 0, \tag{4.24}$$

where the gain α_l ($0 \leq \alpha_l < 1$) is set to a positive value when the signal is judged reliable, and otherwise zero. In order to determine if the l:th segment is reliable, i.e. contains AF, measures based on $\mathbf{q}_l$ and $\hat{\mathbf{q}}_l$ are employed. The segment is accepted as AF if 1) the SNR is sufficiently large, 2) the model error exhibits no sudden decrease, 3) the second largest peak has neither too high a magnitude, nor 4) is too close to the position of the fundamental. The SNR is estimated by the ratio between the average of the fundamental and the first harmonic magnitudes to the noise level between these two peaks.

The criteria for determining if a signal segment is reliable based on its spectrum, was further refined in [56]. Each spectrum $\mathbf{q}_l$ was modeled as a sum of $M+1$ gaussian functions,

$$\psi(f, \boldsymbol{\theta}) = \sum_{i=0}^{M} A_i e^{-\frac{(f-\mu_i)^2}{2\sigma_i^2}} \tag{4.25}$$

where A_i is the magnitude, σ_i is the width, and μ_i is the location of the i:th peak of the spectrum. Since harmonics were expected to be located at integer multiples of f_0, the location of the i:th gaussian was constrained to an interval centered around $i \cdot f_0$, whose width was defined by the frequency shift Δ_i, so that

$$\mu_0 = f_0 \tag{4.26}$$

$$\mu_i = f_0 \cdot i + \Delta_i, \quad i = 1, \ldots, M \tag{4.27}$$

Consequently, the parameter vector $\boldsymbol{\theta}$ was defined by

$$\boldsymbol{\theta} = [\ A_0 \quad \cdots \quad A_M \quad \sigma_0 \quad \cdots \quad \sigma_M \quad f_0 \quad \Delta_1 \quad \cdots \quad \Delta_M\ ]^T. \tag{4.28}$$

The parameters were obtained by minimizing the cost function

$$J_l(\boldsymbol{\theta}) = (\mathbf{q}_l - \boldsymbol{\psi}(\boldsymbol{\theta}))^T \mathbf{D} (\mathbf{q}_l - \boldsymbol{\psi}(\boldsymbol{\theta})) \tag{4.29}$$

where the vector $\boldsymbol{\psi}(\boldsymbol{\theta})$ resulted from evaluation of $\psi(f, \boldsymbol{\theta})$ at the frequencies $f_k = f_0 \cdot 10^{\frac{k}{K}}$, $k = 0, \ldots, K-1$, and $\mathbf{D}$ is a weight matrix designed to compensate for the low-frequency emphasis caused by the logarithmic scaling and to reduce the influence of regions between peaks of the spectrum. The reliability of a signal segment was judged based on its corresponding fitted gaussian model; if 1) no large peak were present in the spectrum between the fundamental and the first harmonic, 2) the spectral concentration of the fundamental was large enough, and 3) the model error was below a certain threshold the segments was used to update the spectral template.

Measures that characterizes the spectral content of the atrial activity may be extracted from the spectral template. A spectral line model is used to

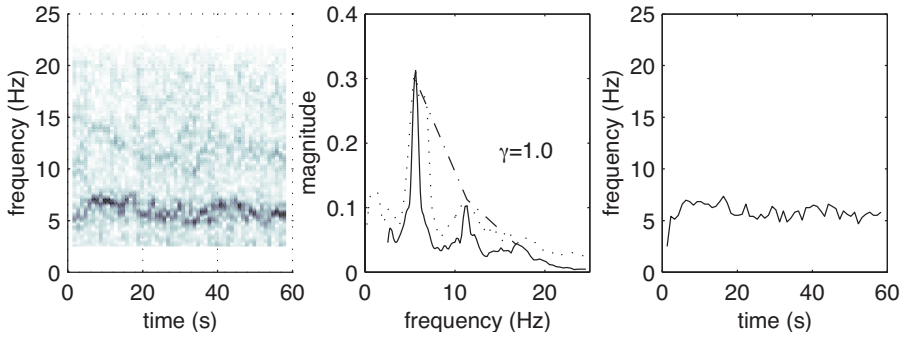

Figure 4.1: Analysis of one minute signals with AF producing a logarithmic STFT (left panel), the spectral template (middle panel) and the AF frequency trend (right panel). Reprinted from [31] with permission.

parameterize $\boldsymbol{\phi}_l$, by means of its magnitudes at the fundamental and harmonics [31].

$$\boldsymbol{\phi}_l(p_l + h_m) = \begin{cases} b_l e^{-\gamma_l m}, & m = 0, 1, \ldots, M \\ 0, & \text{otherwise,} \end{cases} , \tag{4.30}$$

where b_l is the peak magnitude of the fundamental, and γ_l is the exponential decay of each of the M harmonics. The parameter h_m denotes the offset position of the m:th harmonic in relation to the fundamental at p_l. The exponential decay, γ_l, and the peak magnitude, b_l, are estimated by minimizing the least squares cost function using the logarithm of the spectral line model,

$$J(\ln b_l, \gamma_l) = \sum_{m=0}^{M} (\ln \phi_l(p_l + h_m) - (\ln b_l - \gamma_l m))^2. \tag{4.31}$$

The spectral template method is illustrated in Fig. 4.1. Lower values of γ_l has been associated with spontaneous termination of AF [35,54] and lower risk of early AF recurrence following electrical cardioversion [55].

4.2.2 The Phase-Delay Method

The morphology of the f waves can be quantified using the delay between the phase of the fundamental and that of the harmonics [33]. The rationale for this type of analysis is that the morphology of the f waves is believed to reflect the propagation pattern of the impulses in the atria. The atrial activity of the ECG is filtered around the dominant frequency f_0 and the harmonics f_m,

$m = 1, \ldots, M$, respectively, using narrowband filters. The signal component corresponding to each filtered subband of atrial activity is then segmented into nonoverlapping blocks of length L, where each segment is being analyzed separately. The normalized frequencies $f_{m,p}$, and phases $\phi_{m,p}$ are estimated using the following estimators

$$\hat{f}_{m,p} = \arg\max \left| \frac{1}{L} \sum_{n=0}^{L-1} y_{m,p}(n) e^{-j2\pi f n} \right| \tag{4.32}$$

$$\hat{\phi}_{m,p} = \arctan \left(- \frac{\sum_{n=0}^{L-1} y_{m,p}(n) \sin(2\pi \hat{f}_{m,p} n)}{\sum_{n=0}^{L-1} y_{m,p}(n) \cos(2\pi \hat{f}_{m,p} n)} \right) + \frac{\pi}{2}. \tag{4.33}$$

where $y_{m,p}(n)$ is the n:th sample of the p:th block in the m:th harmonic subband of atrial activity. Since the f waves may be irregular within one block, the estimated phase $\hat{\phi}_{m,p}$ is shifted to represent the middle of the block $y_{p,m}$ rather than the beginning, in order to better fit the entire block. Hence,

$$\hat{\phi}'_{m,p} = \hat{\phi}_{m,p} + 2\pi(\hat{f}_{m,p} - m\hat{f}_{0,p})t_m \tag{4.34}$$

where t_m is the time from block onset to middle of the block. In order to compare the phase of the harmonics to that of the fundamental, a scaling operation is performed, so that all phases relate to the same time-scale.

$$\hat{\phi}''_{m,p} = \frac{\hat{\phi}'_{m,p}}{m+1}. \tag{4.35}$$

The phase relationship is finally quantified by subtracting $\hat{\phi}''_{0,p}$ from $\hat{\phi}''_{m,p}$.

$$\hat{\theta}_{m,p} = \hat{\phi}''_{m,p} - \hat{\phi}''_{0,p} \pm l\frac{2\pi}{m+1} \tag{4.36}$$

where l is an integer; the last term is added to adjust $\hat{\theta}_{m,p}$ inside the interval.

The phase relationships of the odd harmonics can be used to quantify symmetry of the f waves, whereas both even and odd harmonic phases relationships contribute to characterize other features of the f wave morphology. This type of detailed morphologic analysis can only be performed on "organized" AF, i.e. with low AF frequency and large harmonics; the method is sensitive to noise, as noise may conceal the harmonics.

4.3 Complexity

Different nonlinear measures have been proposed to quantify the complexity of the atrial activity in the ECG during AF with varying results; the sample

entropy, when applied to a residual ECG which has been filtered in a narrow band around its AF frequency, has proved to be able to predict outcome of electrical cardioversion and spontaneous AF termination [34], whereas other studies have found no correlation between complexity and spontaneous AF termination [35, 57].

4.3.1 Conditional Entropy

The conditional entropy $\mathcal{H}_{CE}$ describes the amount of information conveyed in the most recent sample in a segment of length L when the previous $L-1$ samples are known [58]. It is estimated using Shannon entropy according to

$$\mathcal{H}_{CE}(L) = -\sum p(x_L)\log p(x_L) + \sum p(x_{L-1})\log p(x_{L-1}) \tag{4.37}$$

where $p(x_L)$ is the probability of the sequence $x_L = (x(i), \ldots, x(i+L-1))$ among the $N-L+1$ sequences of length L which may be extracted from the signal $x(n)$, $n = 1, \ldots, N$. A regularity index $\mathcal{H}_R$, which ranges from 0 for white noise to 1 for a periodic signal may be derived from $\mathcal{H}_{CE}(L)$ as follows,

$$\mathcal{H}_R = 1 - \min_L \frac{\mathcal{H}_{CCE}(L)}{E(x)}, \tag{4.38}$$

where $E(x)$ is the process entropy and $\mathcal{H}_{CCE}(L)$ is $\mathcal{H}_{CE}(L)$ corrected to account for finite length signals, using

$$\mathcal{H}_{CCE}(L) = \mathcal{H}_{CE}(L) + p(x_L)E(x). \tag{4.39}$$

This regularity index has been been used to characterize f waves when trying to discriminate between paroxysmal and persistent AF. No significant differences in $\mathcal{H}_R$ were found between the two groups [57].

4.3.2 Sample Entropy

The sample entropy $\mathcal{H}_{SaE}$ compares similarity in fixed length segments of a signal [59]. $\mathcal{H}_{SaE}$ is defined as the negative natural logarithm of the probability of that sequences that are similar for m points remain similar for an additional point. The signal $x(n)$ is divided into different time segments, $\mathbf{x}_m(i)$, of length m, starting at time index i,

$$\mathbf{x}_m(i) = \begin{bmatrix} x(i) & x(i+1) & \cdots & x(i+m-1) \end{bmatrix}^T. \tag{4.40}$$

The distance between two vectors, $\mathbf{x}_m(i)$ and $\mathbf{x}_m(j)$, is calculated as the infinity norm,

$$d(\mathbf{x}_m(i), \mathbf{x}_m(j)) = \max\left(|\mathbf{x}_m(i) - \mathbf{x}_m(j)|\right). \tag{4.41}$$

The number of vectors $\mathbf{x}_m(j)$ within the distance r of vector $\mathbf{x}_m(i)$, $j \neq i$, is denoted A_i. Then, $D_i^m(r)$ represents an estimate of the probability that any segment of length m in the signal is similar to the vector $\mathbf{x}_m(i)$,

$$D_i^m(r) = \frac{A_i^m}{N-m-1}, \tag{4.42}$$

and $D^m(r)$ is the probability that any pair of two vectors of length m are similar,

$$D^m(r) = \frac{1}{N-m} \sum_{i=0}^{N-m-1} D_i^m(r). \tag{4.43}$$

The sample entropy, $\mathcal{H}_{SaE}$, is defined as

$$\mathcal{H}_{SaE}(m,r,N) = -\ln\left(\frac{D^{m+1}(r)}{D^m(r)}\right). \tag{4.44}$$

A high value of $\mathcal{H}_{SaE}$ indicates high complexity of $x(n)$. Sample entropy closely related to approximate entropy [60], but better suited for short noisy data series. Attempts have been made to use sample entropy for prediction of spontaneous termination of AF, but no significant differences were found between non-terminating and terminating AF [35].

A reason for the unsuccessful results obtained in [35] may be that measures of complexity are particularly sensitive to noise. To overcome this problem, Alcaraz et al. [61] proposed to compute the sample entropy of the main atrial wave, i.e. the fundamental waveform of the residual ECG. The main atrial wave can be obtained from the residual ECG, e.g., using wavelet decomposition [61, 62] or by selective narrowband filtering centered around the AF frequency [63,64]. This measure proved to be successful in predicting spontaneous AF termination [61,63,64] as well as the outcome of electrical cardioversion [62]. Figure 4.2 illustrates two residual ECG signals, and the corresponding dominant atrial wave $x_0(n)$ for 10-s segments with paroxysmal and persistent AF, respectively. In this example, the values of both f_0 and $\mathcal{H}_{SaE}$ are much larger for persistent AF than for paroxysmal AF.

A downside with this narrowband filtering approach is that the information contained in the harmonics of the atrial activity is disregarded.

4.4 Spatial Characterization

The spatial characteristics of the atrial activity in the ECG may reflect the propagation of impulses in the atria. Different methods to quantifying spatial characteristics have been proposed, including vector analysis [36,37], and linear mixing models [38].

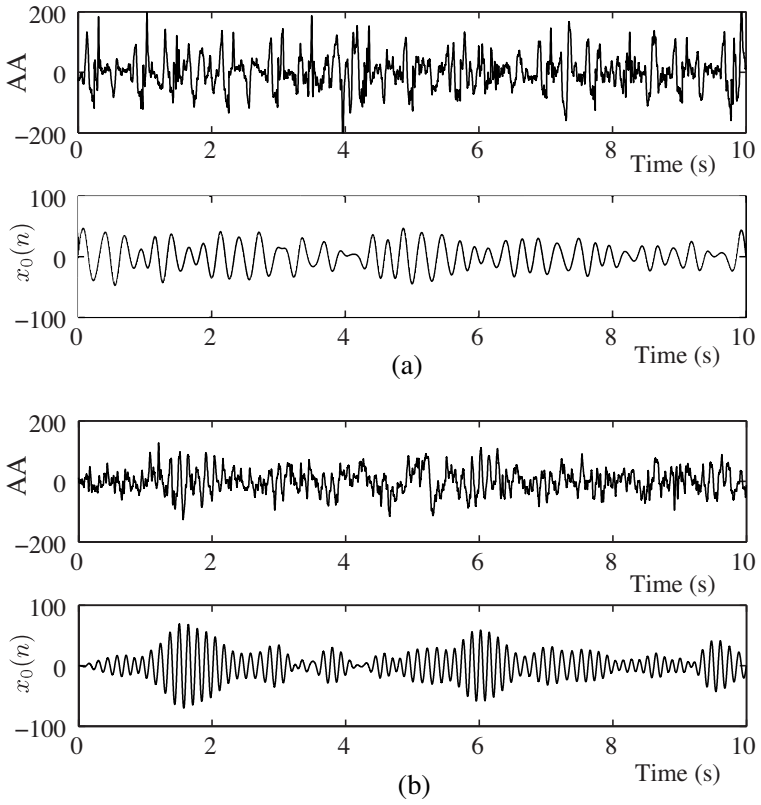

Figure 4.2: Atrial activity (upper panel) and the corresponding dominant atrial wave $x_0(n)$ (lower panel) for (a) paroxysmal AF ($f_0 = 5.65$ Hz, $\mathcal{S}_0 = 0.056$) and (b) persistent AF ($f_0 = 7.35$ Hz, $\mathcal{S}_0 = 0.113$).

4.4.1 Vector Analysis

Vector analysis has been applied to spatially characterize atrial activity of ECG signals during AF and atrial flutter. Three-dimensional vector loops are constructed using ECG signals from orthogonal leads; orthogonal leads can be derived from the standard 12-lead ECG using the inverse Dower transform [65]. Each loop is characterized by its plane of best fit, i.e. the 2-dimensional projection of the loop that produces the minimum mean squared error with respect to the original loop. This plane is determined from eigenanalysis of the covariance matrix that results from the $3 \times N$ data matrix with samples from the 3 orthogonal leads; N denotes the number of samples of each segment.

Eigendecomposition results in the eigenvectors $\mathbf{e}_1$, $\mathbf{e}_2$ and $\mathbf{e}_3$, associated to the eigenvalues $\lambda_1 \geq \lambda_2 \geq \lambda_3$; $\mathbf{e}_1$ and $\mathbf{e}_2$ spans the plane of best fit, while $\mathbf{e}_3$ defines the perpendicular axis.

The perpendicular direction of each plane can be described in terms of azimuth ϕ_{AZ} and elevation ϕ_{EL} angles relative to the frontal plane. These angles can be obtained from the vector $\mathbf{e}_3 = [e_{3x}, e_{3y}, e_{3z}]$, such that

$$\phi_{AZ} = \arctan\left(\frac{e_{3z}}{e_{3x}}\right), \tag{4.45}$$

$$\phi_{EL} = \left|\arctan\left(\frac{e_{3y}}{\sqrt{e_{3x}^2 + e_{3z}^2}}\right)\right|. \tag{4.46}$$

The degree of organization can be quantified by similarity in the planes of best fit obtained from different signal segments; if ϕ_{AZ} was within the same 30 degree region for $> 30\%$ of the segments, it was considered as organized [36]. The spatial stability was compared to the dominant frequency gradient, i.e. the difference between dominant frequencies measured invasively in the left and right atrium, respectively, showing that a high spatial stability corresponded to a low frequency gradient [66].

Each vector loop can also be characterized in terms of planarity ψ_{PL}, i.e. how well a vector loop is fitted to its plane and planar geometry ψ_{PG}, i.e. how circular the vector loop is in its plane of best fit [37]. These measures can be derived from the eigenvalues,

$$\psi_{PL} = \frac{\lambda_3}{\lambda_1 + \lambda_2 + \lambda_3}, \tag{4.47}$$

$$\psi_{PG} = \frac{\lambda_2}{\lambda_1}, \quad \lambda_1 > \lambda_2. \tag{4.48}$$

Figure 4.3 displays an example of vector loops constructed from a 1-s segment of residual ECG. In this example, the azimuth angle indicates that the plane of best fit is in the sagittal plane ($\phi_{AZ} = -23.3°$). The elevation angle ϕ_{EL} is 16.7°. The loops are quite planar ($\psi_{PL} = 0.95$), and have an elliptic appearance ($\psi_{PG} = 0.35$).

4.4.2 Mixing Matrices

The mixing matrix $\mathbf{P}$ obtained using PCA, cf 3.2, has been proposed for determining spatial complexity and temporal stationarity of the atrial activity in surface recordings [38]. In this work, SVD was applied to 10-s segments of the atrial activity of body surface potential maps (BSPM) consisting of $M = 56$ simultaneous recordings.

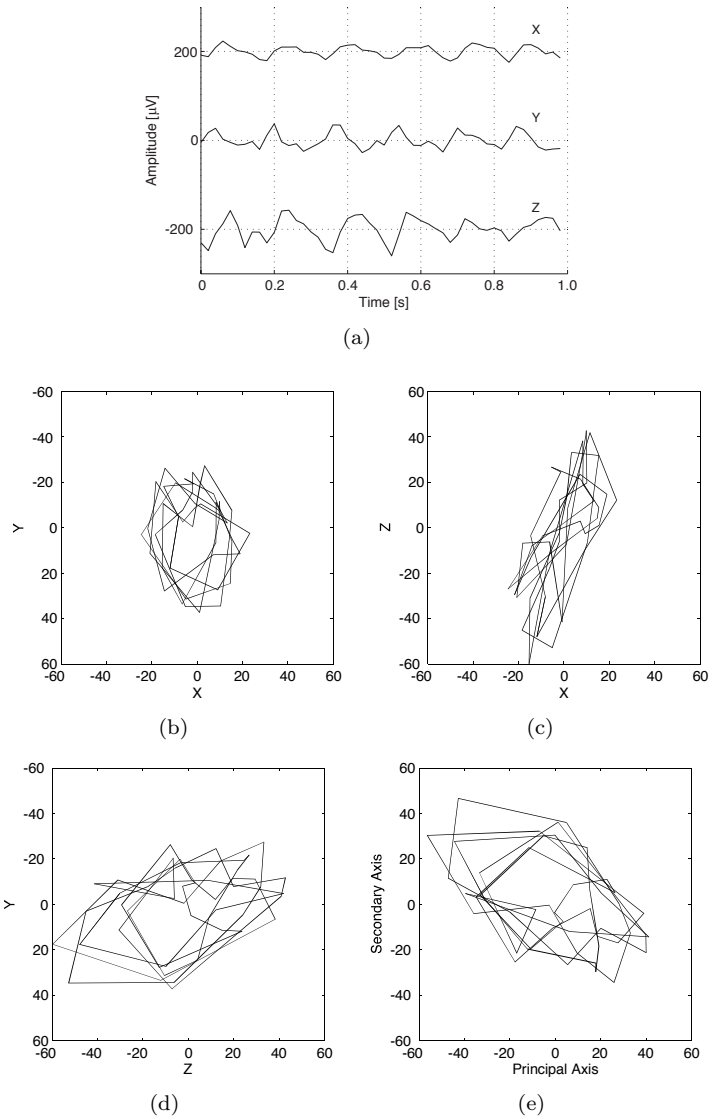

Figure 4.3: Example of a 1-s segment, containing approximately six f waves. (a) The orthogonal leads X, Y, and Z after QRST cancellation. (b) Frontal plane. (c) Transverse plane. (d) Sagittal plane. (e) Plane of best fit. The azimuth angle indicates that the plane of best fit is in the sagittal plane ($\phi_{AZ} = -23.3°$). The elevation angle ϕ_{EL} is 16.7°. The loops are quite planar ($\psi_{PL} = 0.95$), and have an elliptic appearance ($\psi_{PG} = 0.35$). Reprinted with permission from [37].

A larger spatial organization of the atrial activity was assumed to be reflected in terms of a lower number of principal components $\mathbf{y}_i$ needed to accurately represent the signals $\mathbf{x}_i$, $i = 1, \ldots, M$. Accuracy of representation was quantified in terms variance of $\mathbf{x}_i$ captured by the k first principal components $\mathbf{y}_i$, $i = 1, \ldots, k$, and was estimated from the singular values σ_i, $i = 1, \ldots, M$, contained in the matrix $\mathbf{\Sigma}$,

$$v_k = \frac{\sum_{i=1}^{k} \sigma_i^2}{\sum_{i=1}^{M} \sigma_i^2}. \tag{4.49}$$

The number of principal components $k_{0.95}$ required to capture 95% of the signal variance, i.e. $v_k = 0.95$, was used as a measure of spatial complexity.

Temporal stationarity of the atrial activity was quantified by the repetitiveness of the mixing matrix $\mathbf{P}$ along the recording. The k first principal components $\mathbf{y}_i^{(1)}$, $i = 1, \ldots, k$, obtained from the first 10-s segment in a recording were used to reconstruct the signals $\mathbf{x}^{(s)}$ of the following 10-s segments, $s = 2, \ldots, 6$. The normalized mean square error $\epsilon_k^{(s)}$ when reconstructing $\mathbf{x}_{18}^{(s)}$, i.e, the lead of the BSPM with the most prominent atrial activity, based on $\mathbf{y}_i^{(1)}$, $i = 1, \ldots, k$, was used as a measure of temporal stationarity. The error ϵ_k was computed for $k_{0.95}$, determined in the previous step, and for $k = 3$.

Clustering analysis based on the measures $v_{0.95}$, $\epsilon_{k_0.95}$, and $\epsilon_{k=3}$ was applied to separate patients into different groups. The clinical relevance of these parameters has, however, yet to be shown.

Chapter 5

Ventricular Rate during AF

The ventricular rate during AF differs from that during normal sinus rhythm in that it is more irregular and generally more rapid. While the ventricular rate during normal sinus rhythm is determined by the sinus node, the ventricular rate during AF mainly reflects AV nodal properties, e.g., refractoriness and degree of concealed conduction.

5.1 Analysis of Ventricular Rate

In order to obtain the ventricular rate, the QRS complexes need to be detected. This is usually done through a three-step process, consisting of linear filtering to suppress other parts of the ECG signal, a nonlinear transform to enhance the QRS complex, and finally a decision rule to decide whether a QRS complex is present or not [1]. The QRS complexes are also classified according to their morphology, in order to identify so-called ectopic beats which do not originate from the sinus node.

The ventricular activity during AF can be studied through the RR intervals, i.e. the distance between consecutive QRS complexes in the ECG signal. Thus, the interval tachogram, defined as

$$d_{RR,k} = t_k - t_{k-1}, \quad k = 1, \ldots, M, \tag{5.1}$$

where t_k is the fiducial point of the k:th QRST complex, is commonly used in analysis of ventricular activity. Generally, RR intervals preceding and succeeding an ectopic beat are excluded before analysis of the RR interval series.

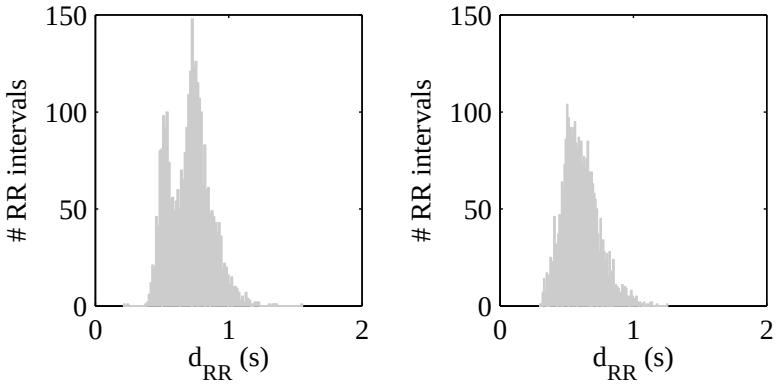

Figure 5.1: RR interval histograms constructed from 30 min of ECG from two patients with AF.

5.1.1 RR Interval Histogram

Analysis of RR interval histograms is basically limited to Holter recordings, since a large number of intervals is needed in order to construct a reliable histogram. The RR interval histogram during normal sinus rhythm is essentially unimodal with a relatively narrow gaussian shape, while the RR interval histogram during AF may exhibit a variety of shapes [67]. Figure 5.1 displays two examples of RR interval histograms during AF.

In about 55% of the patients, the RR interval histogram during AF shows two distinct peaks [68]; the two peaks are believed to correspond to dual AV nodal paths [69–72].

5.1.2 Heart Rate Stratified Histograms

Heart rate stratified histograms (HRSH) can be used to facilitate detection of multiple peaks. In this technique different histograms are constructed based on mean heart rate, in order to reduce smearing caused by fluctuations in heart rate. The ECG signal is divided into segments containing a fixed number of beats, and, for each segment, the mean RR interval is calculated. The segments are grouped according to mean heart rate, and the RR intervals of each group are used to construct a histogram [71, 73].

An example of a bimodal HRSH is displayed in Fig. 5.2. Various measures quantifying the properties of the bimodal histograms can be obtained; the peaks

corresponding to the longest and shortest RR interval population are named slow peak value (PVs) and fast peak value (PVf), respectively. The peak gap (PG) is defined as the distance between the longest and shortest RR population, and the peak value ratio (PVR) is the ratio between the slow and fast peak values. Figure 5.2 illustrates these measures. A problem with this type of analysis, is that the result is dependent on the selection of bins in the histogram. In order to detect peaks in the histogram, smoothing is generally required. This can be arranged, e.g., using a moving average filter with iterative prolongation of window length, repeated until no peaks are closer than 50 ms [71]. However, the results will depend on the method used for histogram smoothing.

5.1.3 Poincaré Plot

Poincaré plots, which are sometimes referred to as Lorenz plots, can be used when analyzing ventricular response during AF. In a Poincaré plot, individual RR intervals are plotted against the corresponding adjacent preceding intervals. Whereas RR interval histograms can only be used to study the distribution of RR intervals, the Poincaré plots displays dependence between two consecutive RR intervals.

The pattern of such plots can be used to distinguish AF from normal sinus rhythm as well as from other supraventricular tachycardias such as atrial flutter. While the Poincaré plot during normal sinus rhythm is centered around the main diagonal, the irregularity of RR intervals during AF results in a widely scattered plot. During atrial flutter clusters are visible in the Poincaré plot as a result of the AV node conducting a periodic number of atrial impulses arriving. Figure 5.3 shows examples of Poincaré plots from normal sinus rhythm, atrial flutter, and AF.

The lower envelope U_{LE} of the Poincaré plot has been used to estimate the functional refractory period of the AV node and its dependence on cycle length [75]. The degree of scatter of the Poincaré plot, estimated by the root mean square difference of each RR interval and U_{LE}, has been used as a measure of the degree of concealed conduction [46].

One method to estimate U_{LE} is by linear regression [76]; the horizontal axis is divided into consecutive bins, and for each bin, the minimal value is detected. The lower envelope is then estimated by line fitting to the minimal values. This method is not robust against outliers, since all points in the Poincaré plot are weighted equally.

Another, more robust method to estimate U_{LE} is by using the Hough transform [77]. This transform has been used for robust detection of shapes, e.g, straight lines, in images. In an (x, y)-space a straight line can be expressed as $y = mx + c$. In the Hough space the straight line is characterized by its slope

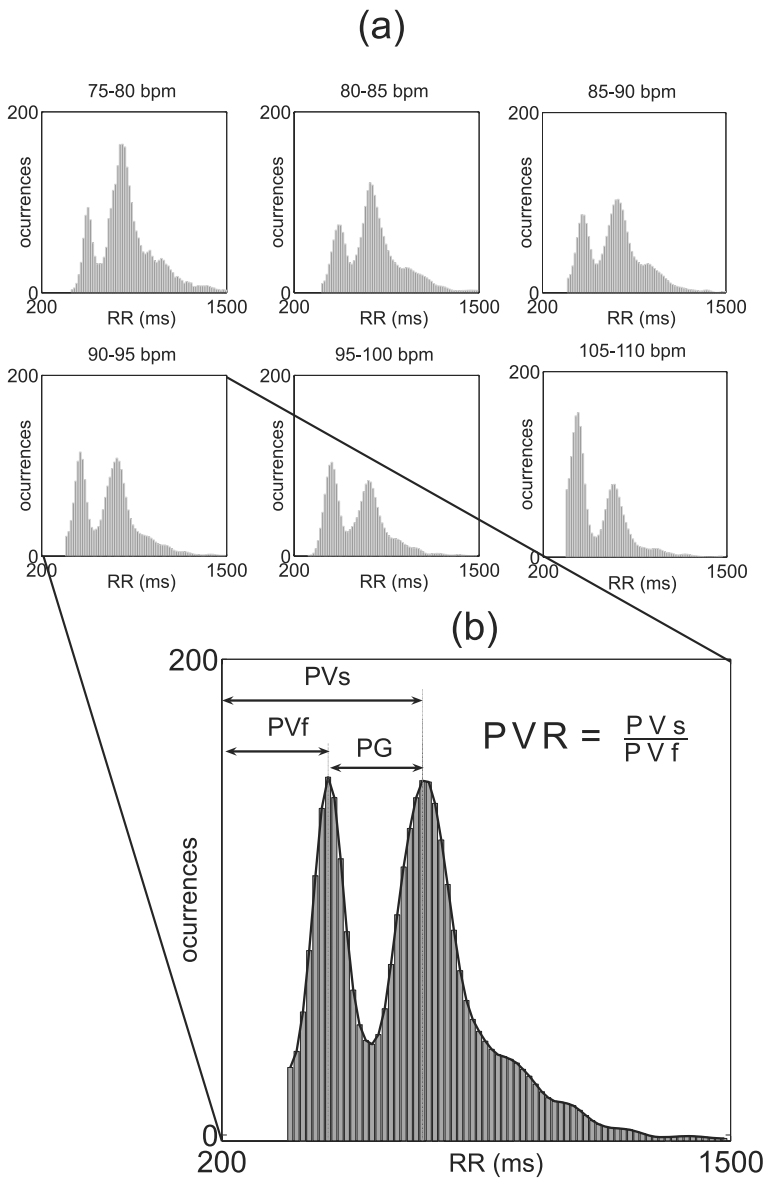

Figure 5.2: (a) Heart rate stratified histograms (HRSH) presenting two RR interval populations, and (b) illustration of measures derived from one of the HRSH. Reprinted with permission from [74].

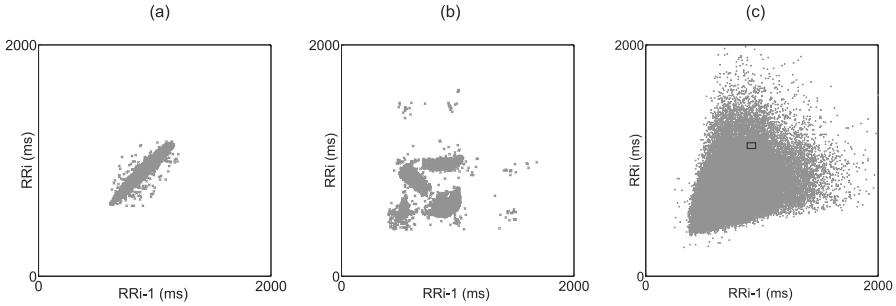

Figure 5.3: Poincaré plots of 24-h recordings of different patients during (a) sinus rhythm, (b) atrial flutter, and (c) AF. Reprinted with permission from [74].

and intercept (m, c). Since (m, c) are unbounded, the line is rather expressed in the pair of parameters (ρ, θ), where ρ is the minimal distance from origo to the line, and θ is the angle from origo to the closest point on the line. Each point (x, y) is expressed by a sinusoidal curve

$$\rho(\theta) = x \cos\theta + y \sin\theta, \quad -\frac{\pi}{2} \leq \theta \leq \frac{\pi}{2}. \tag{5.2}$$

in the Hough space, representing all lines intersecting (x, y). A line in (x, y)-space is characterized by sinusoids $\rho(\theta)$ intersecting at the corresponding value of (ρ, θ) in the Hough space.

When using the Hough transform for estimating U_{LE} of a Poincaré plot, some preprocessing is required. For each value of $d_{RR}(n-1) = x$, there are usually several corresponding $d_{RR}(n)$ values; the minimum $d_{RR}(n) = y$ among these is selected for intervals not exceeding 2 s. Each pair of coordinates (x, y) is then transformed into Hough space. The point in Hough space where the largest number of curves $\rho(\theta)$ intersect, indicated by the coordinates $(\rho_{max}, \theta_{max})$, is converted to (x, y)-space and expressed in terms of slope m and intersect c using

$$(x_0, y_0) = \left(\frac{\rho_{max}}{\cos\theta_{max}}, \frac{\rho_{max}}{\sin\theta_{max}} \right) \tag{5.3}$$

$$(m, c) = \left(-\frac{y_0 - 1}{x_0 - 1}, y_0 \right). \tag{5.4}$$

5.1.4 Histographic Poincaré plots

In a histographic Poincaré plot, each point is associated with the number of occurrences of RR interval pairs given by the coordinates $(d_{RR,k-1}, d_{RR_k})$ [78]. Similar to the peaks of RR interval histograms, the clusters of such a plot may reflect preferential AV node conduction routes.

The diagonal of the histographic Poincaré plot, referred to as the Poincaré surface profile (PSP), can be interpreted as an RR histogram where only RR intervals that were preceded with RR intervals with approximately the same length has been considered [79]. In order to reduce variability caused by RR series of limited length, a two-dimensional lowpass filter was applied to the histographic Poincaré plot, prior to extraction of the PSP. It was concluded that more peaks could be detected using the PSP than using the conventional histogram. A problem with this approach is that the number of RR intervals used to construct the PSP is strongly reduced compared to the original RR series, only about 1/50 of the RR intervals are used; an insufficient number of RR intervals can cause spurious peaks in the histogram.

5.2 AV Modeling

The ventricular response during AF is to a large extent determined by AV nodal blocking of atrial impulses that continuously bombard the AV node. Several functional models of the AV node during AF have been proposed, incorporating various physiological phenomena, e.g., concealed conduction and AV nodal refractoriness. Simulated RR series with different properties can be obtained by changing the model parameters; some models need invasive data as input [80, 81], whereas other models rely on the stochastic properties of atrial impulses arriving to the AV node [67, 82, 83]. Attempts have also been made to estimated model parameters from real data by comparing properties of simulated RR series to the true RR series.

5.2.1 The Cohen Model

In this model, the turbulent atrial activity is assumed to cause atrial impulses arriving randomly to the AV node at a mean rate of λ [67]. The arrival of atrial impulses is statistically characterized by a Poisson process. The AV node is modeled as a lumped structure; the transmembrane potential V_M of the AV node determines when a ventricular activation is triggered. The AV node is refractory to stimulation of atrial impulses during a time period τ from the occurrence of the previous ventricular activation. At the end of the refractory period, V_M is at its resting potential V_R. Spontaneous depolarization causes V_M

to increase at a rate of $\dot{V}_4$. In addition to this spontaneous depolarization, each atrial impulse arriving to the AV node causes an increase of V_M by a discrete amount ΔV. Once V_M has reached a certain threshold V_T, a ventricular beat is initiated. Hence, a ventricular activation occurs when

$$V_M = V_R + n(t)\Delta V + \dot{V}_4 t = V_T, \tag{5.5}$$

where $n(t)$ is the number of atrial impulses that has arrived, and t is the time that has passed since the end of the previous refractory period.

Since atrial impulses are arriving according to a Poisson process, the PDF of the number of atrial impulses n that has arrived at a certain time t after the end of the refractory period is given by

$$p(n) = \frac{e^{-\lambda t}}{n!}. \tag{5.6}$$

Using (5.5) and (5.6), a PDF of the time t from the end of a refractory period to a ventricular activation can be derived as,

$$p(t) = e^{-\lambda t}\lambda^{n+1}\frac{t^n}{n!} + \sum_{k=0}^{N-vt} e^{-\lambda t}\frac{(\lambda t)^k}{k!} \cdot \delta\left(t - \frac{N-k}{v}\right), \tag{5.7}$$

where

$$v = \dot{V}_4/\Delta V \tag{5.8}$$

$$N = \frac{V_T - V_R}{\Delta V}, \tag{5.9}$$

and $\delta(\cdot)$ is the impulse function. The time between two consecutive ventricular activations, i.e. an RR interval, is determined by t as well as by the refractory period length τ, so that the i:th RR interval is given by $d_{RR,i} = t_i + \tau_i$. Hence, the PDF of $d_{RR,i}$ can be obtained by right shifting $p(t)$, so that

$$p(d_{RR,i}) = p(t_i - \tau_i). \tag{5.10}$$

The refractory period τ_i is assumed to depend on the previous RR interval length

$$\tau_i = \tau_\infty\left(1 - e^{\frac{-d_{RR,i-1}}{\tau_\infty}}\right), \tag{5.11}$$

such that a longer RR interval is followed by a longer refractory period; τ_∞ is a design parameter of the model.

RR interval series with unimodal as well as bi- and multimodal PDFs can be generated using this model. Attempts were made to estimate the model parameters from RR series of ECGs; the atrial activity was disregarded. However,

the parameter estimates sometimes assumed unphysiological values. Another problem with this model is that several parameter settings can produce a similar RR series, and hence, for some RR series no unique set of parameters can be determined.

5.2.2 The Jørgensen Model

The output sequence of ventricular activations is, in this more recent model [80], predicted on a beat-to-beat basis given an input sequence of atrial activations.

All atrial impulses arriving to the AV node are assumed to cause a ventricular activation unless the AV node is refractory. The AV node is assumed to be refractory during a time period τ_0 following a ventricular activation. Concealed conduction is incorporated in this model, so that each atrial impulse arriving to the AV node while it is refractory causes a prolongation of τ_0 by a fixed time Δ. Hence, the refractory period after the k:th concealed atrial impulse following a conducted atrial impulse is given by

$$\begin{aligned} \tau(k) &= \tau(k-1) + \Delta \\ &= \tau_0 + k \cdot \Delta. \end{aligned} \tag{5.12}$$

The refractory period is reset to τ_0 following each conducted beat.

The AV delay t_{AV}, i.e. the time from that the AV node is depolarized to a ventricular activation is initiated, is also incorporated in this model. The AV delay is assumed to depend on the recovery time t_{RT}, i.e. the time from the end of the preceding refractory period to the arrival of the current atrial impulse, so that a shorter t_{RT} is followed by a longer t_{AV},

$$t_{AV}(k) = t_{AV_{min}} + \alpha e^{-\frac{t_{RT}(k)}{\tau_c}}. \tag{5.13}$$

Thus, the minimal AV delay $t_{AV_{min}}$ occurs when $t_{RT} = 0$, while the maximal AV delay prolongation α occurs when $t_{RT} \to \infty$. The parameter τ_c is the conduction-curve time constant. The model parameters were estimated, using an ad hoc procedure, by comparing recorded RR interval series to the corresponding predicted RR series obtained using different model parameter settings $[\tau_0, \Delta, t_{AV_{min}}, \alpha, \tau_c]$. Since invasive recordings are needed to estimate the parameters of this model, it was only tested on two patients; one in AF and one in atrial flutter.

The model was later modified to account for concealed conduction causing variable refractory period increments $\Delta(k)$ [81]. Here, the refractory period prolongation is defined as

$$\Delta(k) = \Omega(k)\Delta_{std} + \Delta_{mean}, \tag{5.14}$$

where Δ_{mean} and Δ_{std} are the mean value and standard deviation of the refractory period prolongation, and $\Omega(k)$ zero-mean, unit-variance normally distributed random value. Three of the model parameters $[\alpha, \tau_c, \Delta_{std}]$ were fixed, and the remaining parameters $[\tau_0, \Delta_{mean}, t_{AV_{min}}]$ were estimated by grid search in parameter space. For each parameter setting an RR series was generated based on the recorded series of atrial activations. The parameters corresponding to the RR series which was most similar to the recorded RR series in terms of distribution, i.e., yielded the highest significance in a Kolmogorov-Smirnov test, were chosen. This extended model was used to evaluate drug effects in 10 patients with paroxysmal AF; the signals were recorded after open-heart bypass surgery. The results showed that patients treated with amiodarone had increased refractoriness, i.e. τ_0, and concealed conduction, Δ_{mean}, whereas patients treated with β-blockers had an increase in τ_0 and the minimum conduction time $t_{AV_{min}}$.

5.2.3 The Rashidi Model

Atrial impulses are assumed to arrive to the AV node randomly according to a gaussian distribution in this simulation model [82]. The refractory period of the AV node τ was assumed to be limited to 0.3–0.9 s. If the AV node was refractory, the atrial impulses were blocked and the refractory period was increased. The refractory period $\tau(k)$ following a conducted atrial impulse k is initially set to 0.3 s. For each atrial impulse that is blocked, the refractory period is increased according to

$$\tau(k+1) = \tau(k) + u(k)(0.9 - \tau(k)). \tag{5.15}$$

The prolongation of the refractory period is dependent on the time $t(k)$ from the previous conducted atrial impulse and the design parameters a and b, such that

$$u(k) = \frac{1}{1 + e^{-a(z(k)-b)}}, \tag{5.16}$$

where

$$z(k) = \frac{\tau(k) - t(k)}{\tau(k)}. \tag{5.17}$$

Hence, an atrial impulse arriving close in time to a conducted atrial impulse increases the refractory period more than an atrial impulse arriving later. Since the blocked atrial impulses increases the refractory period towards its upper limit, i.e. 0.9 s, a longer refractory period is effected less than a short refractory period. By changing a and b various shapes of the RR interval histograms can be obtained, however, these two parameters have no physiological interpretation.

5.2.4 The Lian Simulation Model

Similar to [67], atrial impulses are assumed to arrive to the AV node according to a Poisson process. In this work, however, the Poisson process is truncated so that the time between consecutive atrial impulses are at least 50 ms, to impose a certain minimal repolarization time of the atria [83]. The atrial impulses are assumed to have different strength, so that ΔV can take on different values. A functional dependence of the AV delay on the recovery time, similar to that used in [80], cf. (5.13) is incorporated in the model.

The refractory period is assumed to depend on the recovery time t_{RT}, so that

$$\tau(k) = \tau_{min} + \beta(1 - e^{-\frac{t_{RT}(k-1)}{\tau_r}}), \tag{5.18}$$

where τ_{min} is the shortest AV refractory period, corresponding to $t_{RT} = 0$, β is the maximum prolongation of the refractory period when $t_{RT} \to \infty$, and τ_r is the refractory curve time constant.

The effect of concealed conduction is incorporated in the model; the refractory period prolongation is assumed to depend on both timing and strength of the blocked impulse, so that

$$\tau'(k) = \tau(k) + \tau_{min} \left(\frac{t}{\tau}\right)^{\theta} \left[max(1, \frac{\Delta V}{V_T - V_R})\right]^{\delta}, \tag{5.19}$$

where t is the time when the impulse is blocked, and θ and δ are parameters modeling the respective dependence of timing and strength on prolongation of the refractory period. The maximal prolongation τ_{min} occurs when a suprathreshold impulse, i.e., $\Delta V > (V_T - V_R)$ arrives at the AV node at the end of the refractory period. The prolongation will be shorter if the impulse arrives earlier or is weaker in strength.

The model was later extended to include the effects of dual chamber pacing [84]. These detailed simulation model is not suited for estimation of parameters from real data.

Chapter 6

Summary of Included Papers

6.1 Paper I: Predicting Spontaneous Termination of Atrial Fibrillation using the Surface ECG

Extracting features that characterizes AF from the surface ECG is important when trying to help physicians diagnosing the arrhythmia. Several features that characterizes the signal may be extracted, but it is also of great interest to know if a feature has some relevance for diagnosing AF. The purpose of this work was to extract features from AF that could predict spontaneous termination. Time-frequency measures, such as amplitude, harmonics decay and frequency, as well as complexity measures were studied.

A database of 80 one-minute segments extracted from 20-24 hour two-channel Holter ECG recordings, sampled at 50 Hz, provided by Physionet [85] for the CinC Challenge 2004 [86], was used in the study. The signals was classified as either non-terminating (N), soon-terminating (S) or immediately terminating (T). The database was divided into a training set of 30 recordings (10N, 10S and 10T), and two test sets with 30 recordings (N and T) and 20 recordings (S and T), respectively.

Preprocessing of the signals consisted of baseline wander and 50 Hz filtering. The atrial activity of the ECG signal was extracted using spatiotemporal QRST cancellation.

Using the spectral template method [31], the AF frequency f_l, fibrillation

Table 6.1: Mean value and standard deviation of measures used for AF characterization, for the non-terminating (N) and immediately-terminating (T) signals in the training set. Measures with boldface asymptotic p-values are significantly different according to a Kolmogorov-Smirnov test.

Parameter average	N $Mean \pm Std$	T $Mean \pm Std$	Asymptotic p-value
$\bar{f}$	6.91 ± 0.66	5.00 ± 0.65	**0.000033**
$\bar{\gamma}$	1.29 ± 0.27	0.79 ± 0.20	**0.0021**
σ_f	0.80 ± 0.23	0.52 ± 0.13	**0.0127**
$\bar{a}$	21.7 ± 12.4	28.6 ± 16.7	N.S.
$\mathcal{H}_{SpE}$	1.73 ± 0.34	1.73 ± 0.18	N.S.
$\mathcal{H}_{SaE}$	1.51 ± 0.34	1.63 ± 0.16	N.S.
$\mathcal{H}_{FSR}$	0.16 ± 0.04	0.14 ± 0.02	N.S.

amplitude a_l, and exponential decay γ_l was obtained for each segment l of 128 samples (2.56 s). A validity measure was employed to check if the segments did contain atrial activity or not. Once occasional episodes of sinus rhythm and local noise had been excluded by the validity parameters, the f_l, a_l, and γ_l of the remaining segments were averaged producing reliable averages of the AF frequency, $\bar{f}$, the exponential decay, $\bar{\gamma}$, and the peak amplitude, $\bar{a}$. The variation of the AF frequency was quantified by the standard deviation σ_f. If more than 75% of the signal segments were invalid, the entire recording was excluded from further analysis.

Three different complexity measures: spectral entropy $\mathcal{H}_{SpE}$, sample entropy $\mathcal{H}_{SaE}$, and fractional spectral radius $\mathcal{H}_{FSR}$ were also examined. The spectral entropy, $\mathcal{H}_{SpE}$, quantifies the spectral complexity of a signal, $x(n)$, and is obtained by applying Shannon's entropy to the PDF of the signal [87]. A large value of $\mathcal{H}_{SpE}$ indicates high complexity of $x(n)$. The sample entropy, $\mathcal{H}_{SaE}$, compares similarity in fixed length segments of the signal [59]. A large value of $\mathcal{H}_{SaE}$ indicates high complexity of $x(n)$. The fractional spectral radius, $\mathcal{H}_{FSR}$, is another measure of complexity which gives an upper bound to the trajectory dimension [87]. A small value of $\mathcal{H}_{FSR}$ indicates a large trajectory dimension, and hence high complexity of $x(n)$.

The features were compared for the different groups of the training set. We found that the mean AF frequency, the variance of the AF frequency and the exponential decay significantly differed between the non-terminating (N) and the terminating (T) AF patients, as shown in Table 6.1. Neither the fibrillation amplitude nor the complexity measures differed between the two groups.

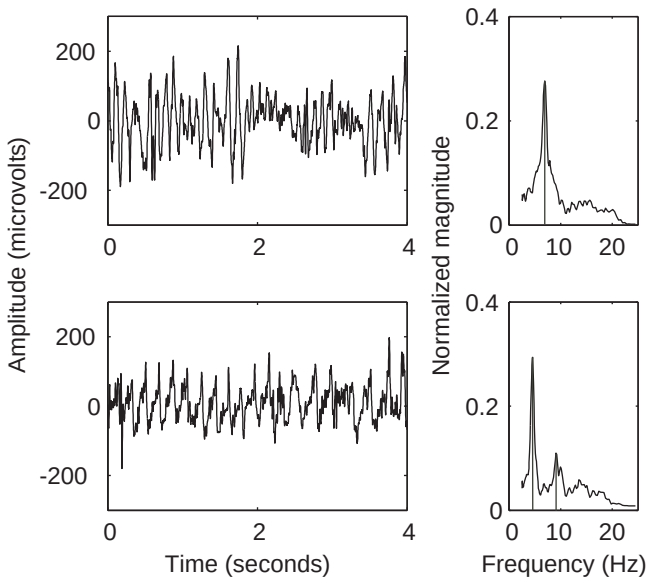

Figure 6.1: Residual ECG signals (left) with different exponential decay, $\bar{\gamma}$, AF frequency, $\bar{f}$, and variation of AF frequency, σ_f and corresponding spectral template, $\boldsymbol{\phi}_l$ (right). (a) Non-terminating AF with $\bar{\gamma} = 1.6$, $\bar{f} = 7.6$ Hz and $\sigma_f = 0.9$, and (b) terminating AF with $\bar{\gamma} = 0.7$, $\bar{f} = 5.0$ Hz, $\sigma_f = 0.4$.

Figure 6.1 shows examples with residual ECG signals of non-terminating and terminating AF and their corresponding spectral template, from which the significant parameters are derived.

There were no significant differences between any of the measures obtained from the soon-terminating (S) and the immediately-terminating (T) signals of the training set, see Table 6.2.

The three significant features were highly correlated. Hence, only the most significant feature, $\bar{f}$, was used to predict possible oncoming spontaneous termination. Using this predictor, 90% of the test set was correctly classified into N and T.

Table 6.2: Mean value and standard deviation of measures used for AF characterization, from the soon-terminating (S) and immediately-terminating (T) signals in the training set.

Parameter average	S $Mean \pm Std$	T $Mean \pm Std$	Asymptotic p-value
f	5.33 ± 0.65	5.00 ± 0.65	N.S.
$\bar{\gamma}$	0.90 ± 0.17	0.79 ± 0.20	N.S.
σ_f	0.67 ± 0.32	0.52 ± 0.13	N.S.
$\bar{a}$	32.3 ± 17.8	28.6 ± 16.7	N.S.
$\mathcal{H}_{SpE}$	1.74 ± 0.16	1.73 ± 0.18	N.S.
$\mathcal{H}_{SaE}$	1.61 ± 0.12	1.63 ± 0.16	N.S.
$\mathcal{H}_{FSR}$	0.16 ± 0.03	0.14 ± 0.02	N.S.

6.2 Paper II: Frequency tracking of Atrial Fibrillation using Hidden Markov Models

Erroneous AF frequency estimates is a problem, particularly in ambulatory ECG recordings (Holter), where the signal often is corrupted by noise. The purpose of this study was to make AF frequency trend estimation more robust to noise, by post-processing the frequency estimates using a hidden Markov model (HMM) which make use of a priori knowledge of the AF characteristics.

In this approach, given an observed sequence of frequency estimates, $\mathbf{z} = [z(1), z(2), \ldots, z(T)]^T$, our goal is to obtain the true sequence, denoted $\mathbf{x} = [x(1), x(2), \ldots, x(T)]^T$. The HMM for frequency tracking includes one zero state, $z(t) = 0$, when no signal is present, and $P-1$ different frequency states, $z(t) = 1, \ldots, P-1$, where state i includes frequencies between f_i and $f_{i+1} = f_i + \Delta f$, with a center frequency of $\tilde{f}_i$,

$$\tilde{f}_i = f_i + \frac{\Delta f}{2}. \tag{6.1}$$

An HMM is completely characterized by a state transition matrix $\mathbf{A}$, an observation matrix $\mathbf{B}$, and an initial state vector $\boldsymbol{\pi}$ [88].

The $P \times P$ state transition matrix $\mathbf{A}$ describes the transition probabilities between different states; element a_{ij} is the probability that state $x(t+1) = j$ if state $x(t) = i$. It is assumed the changes in AF frequency are characterized by a gaussian PDF, i.e., the AF frequency is more likely to remain the same or to change gradually, than to change drastically. A state transition matrix $\mathbf{A}$ is derived, where the design parameters d, u, and v corresponds to the std of

the gaussian PDF, and the probability of initiation and termination of an AF signal, respectively.

The $P \times P$ observation matrix $\mathbf{B}$ describes the probabilities of observing a specific state given the true state. Its elements, b_{ij}, corresponds to the probability of detection in state j when the true state is i. It is assumed that the observed signal consists of a sinusoid with $K-1$ harmonics and additive noise, according to the following model

$$s(n) = \sum_{k=1}^{K} \alpha_k \sin(2\pi k f_0 n) + w(n). \tag{6.2}$$

The amplitude of the signal, α_1, and its harmonics, $\alpha_2, \ldots, \alpha_K$, and the frequency f_0 is assumed to be constant during the time interval for the Fourier transform; the noise $w(n)$ is assumed to be zero-mean, gaussian with variance σ^2. Setting the design parameters defined by $\alpha_1, \ldots, \alpha_K$, σ^2, and the detection threshold D, an observation matrix $\mathbf{B}$ may be derived.

Given an observed sequence, $\mathbf{z}$, an optimal sequence, $\mathbf{x}$, with respect to $\mathbf{A}$, $\mathbf{B}$ and $\boldsymbol{\pi}$ can be obtained using the Viterbi algorithm [89].

Simulated AF mixed with real noise obtained from ECG recordings as well as white noise to different SNR were used in the evaluation. The frequency estimates were calculated using STFT. An example of frequency tracking using HMM of simulated AF mixed with noise obtained from a real ECG recording to different SNR is displayed in Fig. 6.2. At 10 dB SNR, all frequencies were correctly estimated by the STFT, thus using the HMM has no effect. At 5 dB SNR, two erroneous frequency estimates were excluded and two erroneous frequency estimates were replaced using the HMM. At 0 dB SNR several erroneous estimates were either excluded or replaced using the HMM.

The performance of the HMM method was compared to that of the spectral template method [31]. An average RMS error of the frequency estimates was obtained using four different frequency trends, modeling various types of frequency variation. The average RMS error of the estimated frequencies of simulated AF signals mixed with noise obtained from real ECG recordings is presented in Fig. 6.3. A high zero state occupancy percentage tend to give a lower average RMS error, since the error is undefined at zero state. Therefore, it is important to compare not only the average RMS error, but also the zero state occupancy percentage. As indicated in Fig. 6.3, the average RMS error and the zero-state occupancy is significantly lower for the HMM method than for the spectral template method. Hence, frequency tracking using HMM is particularly suited for signals with large amplitude noise.

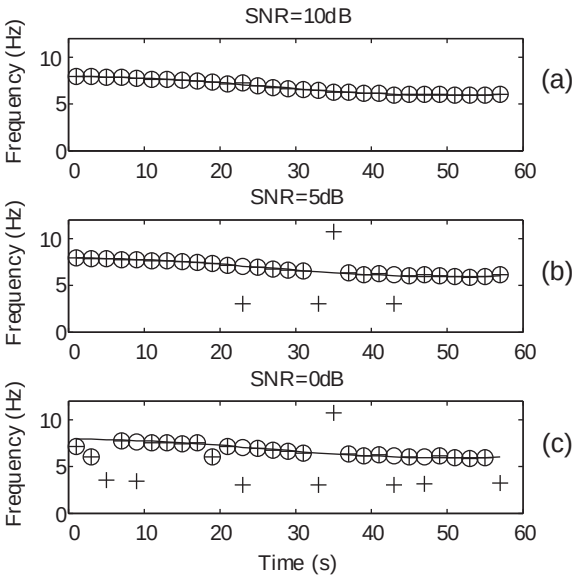

Figure 6.2: Frequency tracking with and without employing the HMM of simulated AF signals mixed with QRST-noise to (a) 10 dB SNR, (b) 5 dB SNR and (c) 0 dB SNR. The true frequency trend (solid line), the estimated frequency using STFT ('+'), and the estimated frequency using HMM ('o'). Note that an absent '+' or 'o' corresponds to zero state.

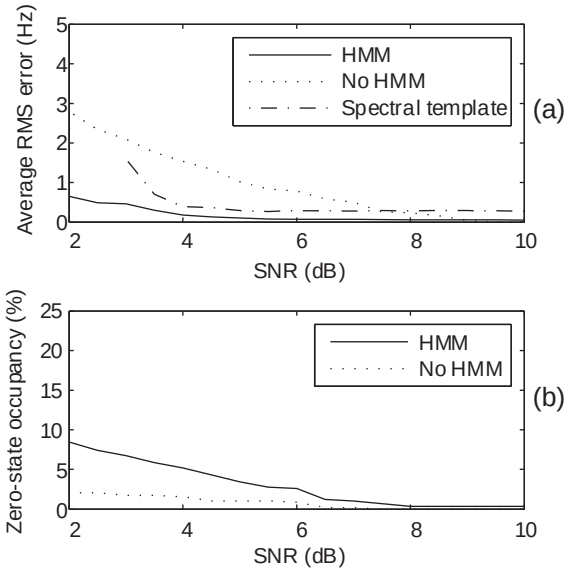

Figure 6.3: (a) RMS error and (b) zero state occupancy as function of SNR for simulated AF with QRST remainders. 'No HMM' denotes use of STFT without HMM.

6.3 Paper III: Circadian Variation in Dominant Atrial Fibrillation Frequency in Persistent Atrial Fibrillation

The purpose of this study was to investigate the dominant AF frequency trend $x_m(n)$ with respect to the presence of circadian variation. Circadian variations are important to study as knowledge about them may help to establish proper timing of drug administration (chronotherapy).

Three different methods were used to quantify circadian variation in AF frequency trends of 18 patients with long-standing persistent AF, obtained from 24-h ECG recordings using HMM-based frequency tracking [90]. Whereas previous studies on circadian variation in AF frequency have been based on sparse measurements [47,48], this study is based on continuous measurements.

First, in the cosinor method [91–93], a sinusoid with 24-hour periodicity, defined by

$$y_m(n) = a_m + b_m \cos\left(\frac{2\pi(n - n_{0,m})}{24}\right), \tag{6.3}$$

was fitted to each frequency trend, resulting in estimates of the magnitude b_m and phase $n_{0,m}$ of the circadian variation. A goodness-of-fit measure γ_m^2 indicating how well the variation in $x_m(n)$ is explained by the fitted curve $y_m(n)$ was also computed. This measure is defined as the ratio between the variance of $y_m(n)$ and the variance of $x_m(n)$, i.e.

$$\gamma_m^2 = \frac{\sum_{n=1}^{N_m}(y_m(n) - \bar{x}_m)^2}{\sum_{n=1}^{N_m}(x_m(n) - \bar{x}_m)^2}, \tag{6.4}$$

where $\bar{x}_m$ denotes mean AF frequency. The measure γ_m^2 can take on values between 0 and 1 where larger values indicate a better fit.

In contrast to the cosinor method, the autocorrelation method [94] does not impose a functional structure on the circadian variation. In this method the autocorrelation function of each AF frequency trend, defined by

$$\hat{r}_m(k) = \frac{1}{N_m}\sum_{n=1}^{N_m-k}(x_m(n) - \bar{x}_m)(x_m(n+k) - \bar{x}_m), \tag{6.5}$$

is used to detect circadian variation. When $x_m(n)$ exhibits circadian variation, $r_m(k)$ has a U-shaped appearance, i.e., the autocorrelation is positive-valued at

0 and 23 hour lags and negative-valued at some intermediate lags. The autocorrelation function $r_m(k)$ is compared to the autocorrelation function $r_{w,m}(k)$ that corresponds to white noise only; $r_m(k)$ is judged to reflect circadian variation if it differs significantly from $r_{w,m}(k)$.

Finally, in the ensemble correlation method, variations of the frequency trends of the different recordings are time-aligned and averaged to reveal joint variational patterns [1].

$$\mu_{\Delta x}(n) = \frac{1}{M} \sum_{m=1}^{M} \Delta x_m(n), \tag{6.6}$$

where

$$\Delta x_m(n) = x_m(n) - \bar{x}_m \tag{6.7}$$

and M is the number of frequency trends. A weighting factor $w(n)$ is derived from the ensemble correlation $\hat{\rho}(n)$, defined by

$$\hat{\rho}(n) = \frac{\sum_{i=1}^{M} \sum_{j=1, i \neq j}^{M} \Delta x_i(n) \Delta x_j(n)}{(M-1) \sum_{i=1}^{M} \Delta x_i^2(n)}, \tag{6.8}$$

such that samples with a large correlation across the ensemble are assigned a larger weight and vice versa [95].

Using the autocorrelation method, circadian variation was found in 13 out of the 18 frequency trends. Using cosinor analysis, the amplitude b_m of the variation was found to be 0.15 ± 0.09 Hz (range $0.05 - 0.30$ Hz), and the acrophase $n_{0,m}$ was found to typically occur in the afternoon or evening (median time was at 15h48). The goodness of fit γ_m^2 of the sinusoid to the observed trend was 0.15 ± 0.13 (range $0.008 - 0.446$), indicating that only a small portion of the variation in AF frequency is accounted for by the fitted sinusoids. The upper frequency trend in Fig. 6.4 (case #1) corresponds to the recording with the largest value of b_m, possibly indicative of circadian variation, whereas the lower frequency trend in Fig. 6.4 (case #2) corresponds to the smallest value.

The ensemble average of the deviations from the mean AF frequency, and the related ensemble correlation are presented in Fig. 6.5 as functions of the time of the day. It is evident from Fig. 6.5(a) that the highest mean AF frequency occurs in the afternoon (about 15h to 17h), while the lowest occurs late in the night (about 1h to 6h). These two periods of the day are associated with the most pronounced joint variation as reflected by the ensemble

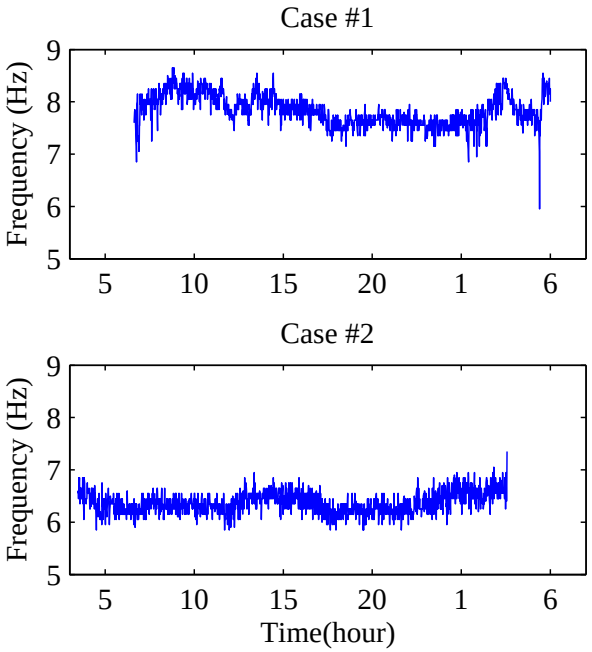

Figure 6.4: Two examples of AF frequency trends corresponding to (a) the largest b_m and (b) the smallest b_m.

correlation, see Fig. 6.5(b). The magnitude of the ensemble average variation is approximately ± 0.15 Hz.

It is concluded that circadian variation is present in most patients with long-standing persistent AF though the short-term variation in AF frequency is considerable and should be taken into account.

6.4 Paper IV: Classification of Paroxysmal and Persistent Atrial Fibrillation in Ambulatory ECG Recordings

The primary question of this study can be formulated as "Given an arbitrarily chosen 10-s segment of an ambulatory ECG recording, which performance can be achieved with respect to classification of paroxysmal and persistent AF?" This question is addressed by investigating the performance of a novel method

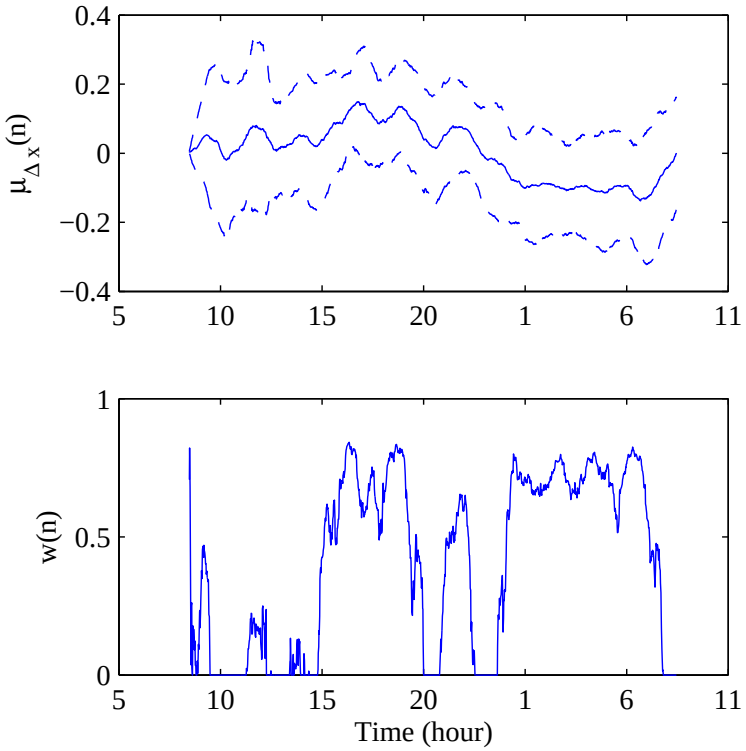

Figure 6.5: (a) The ensemble average (solid line) ± one standard deviation (dashed line) of the deviations from the mean AF frequency $\mu_{\Delta x}(n)$ and (b) the corresponding ensemble correlation $w(n)$.

that makes use of information on harmonics of the atrial signal, derived by a signal-dependent filter bank, and by comparing its performance with existing techniques. A total of 50 patients with 24-h ambulatory ECG recordings were enrolled in the study; 26 patients had paroxysmal AF, whereas the remaining 24 patients had persistent AF. This study differs from Paper I in that a new method is employed to characterize the atrial activity, and that a very much larger database is used. Whereas 1-min excerpts of ECG were used in the studies following the CinC Challenge 2004 [35, 96–100] , entire recordings are analyzed on a 10-s basis in this study.

Following spatiotemporal QRST cancellation, the AF frequency f_0 was tracked on a segment to segment basis, using HMM-based frequency track-

ing [90]. Hence, for each 10-s segment l, a new frequency estimate $f_{0,l}$ was obtained.

Characterization of AF was based on subbands of the atrial activity, corresponding to the fundamental and the first and second harmonic, respectively. These signals, denoted $x_0(n)$, $x_1(n)$, and $x_2(n)$, were obtained using time-varying bandpass filtering of the atrial activity. For each segment l, new filters $H_{0,l}(z)$ $H_{1,l}(z)$, and $H_{2,l}(z)$ with 3 Hz bandwidth, and center frequencies of $f_{0,l}$, $f_{1,l} = 2f_{0,l}$, and $f_{2,l} = 3f_{0,l}$, respectively, were designed and applied to forward/backward filtering of the atrial activity segments; care was taken to minimize transients at the segment boundaries by matching the initial conditions.

Atrial organization was estimated by sample entropy, which examines a signal for similar sequences and assigns a non-negative number to the signal so that larger values correspond to higher complexity [59], cf 4.3.2. The sample entropy was computed for each of the subbands, i.e., $x_{0,l}(n)$, $x_{1,l}(n)$, and $x_{2,l}(n)$, and denoted $\mathcal{S}_{0,l}$ $\mathcal{S}_{1,l}$, and $\mathcal{S}_{2,l}$, respectively. The parameter values were set to $m = 2$, $r = 0.35 \cdot \mathrm{std}(x_{i,l}(n))$, and $N = 10000$, i.e. 10 s at sampling rate 1 kHz [101]. Since the sample entropy does not convey any information on the strength of the harmonics, the relative subband energy a_l of the first and second harmonics was also considered for classification.

The mean and standard deviation of $\mathcal{S}_0$, $\mathcal{S}_1$, $\mathcal{S}_2$, a, and f_0 were determined from all values that resulted from the 10-s segments in patients with either paroxysmal AF (PA) or persistent AF (PE), see Table 6.3. The results show that PA is associated with lower sample entropy, larger harmonics as reflected by a, and lower dominant atrial frequency than PE.

Table 6.3: Parameter values of 10-s segments of paroxysmal AF and persistent AF.

Parameter	Paroxysmal AF Mean±Std	Persistent AF Mean±Std	p-value
$\mathcal{S}_0$	0.085±0.010	0.110±0.016	< 0.0005
$\mathcal{S}_1$	0.192±0.025	0.248±0.038	< 0.0005
$\mathcal{S}_2$	0.285±0.040	0.356±0.047	< 0.0005
a	0.245±0.112	0.157±0.081	< 0.0005
f_0 (Hz)	5.65±0.69	6.73±0.85	< 0.0005

The features of each segment l; the subband sample entropies $\mathcal{S}_{0,l}$, $\mathcal{S}_{1,l}$, and $\mathcal{S}_{2,l}$, the relative harmonics energy a_l, and the dominant atrial frequency f_0,

were grouped into the following four vectors:

$$\mathbf{y}_{1,l} = \left[\mathcal{S}_{0,l}\right], \quad \mathbf{y}_{2,l} = \begin{bmatrix}\mathcal{S}_{0,l}\\ \mathcal{S}_{1,l}\\ \mathcal{S}_{2,l}\end{bmatrix},$$
$$\mathbf{y}_{3,l} = \begin{bmatrix}\mathcal{S}_{0,l}\\ a_l\end{bmatrix}, \quad \mathbf{y}_{4,l} = \left[f_{0,l}\right].$$

The reason for studying these groups was that both $\mathbf{y}_{2,l}$ and $\mathbf{y}_{3,l}$ extend $\mathbf{y}_{1,l}$ with information on the harmonics, though in quite different ways. For comparison, $f_{0,l}$ was included since its significance has been investigated in numerous studies.

For each feature vector $\mathbf{y}_{i,l}$, minimum-error-rate classification with discriminant functions was employed, assuming that the feature vectors were gaussian [102]. Hence, the discriminant functions for PA and PE, designed for the i:th feature vector, are given by

$$g_{PA_i}(\mathbf{y}_{i,l}) = -\frac{1}{2}(\mathbf{y}_{i,l} - \boldsymbol{\mu}_{PA_i})^T \boldsymbol{\Sigma}_{PA_i}^{-1}(\mathbf{y}_{i,l} - \boldsymbol{\mu}_{PA_i}) - \frac{1}{2}\ln|\boldsymbol{\Sigma}_{PA_i}|, \tag{6.9}$$

$$g_{PE_i}(\mathbf{y}_{i,l}) = -\frac{1}{2}(\mathbf{y}_{i,l} - \boldsymbol{\mu}_{PE_i})^T \boldsymbol{\Sigma}_{PE_i}^{-1}(\mathbf{y}_{i,l} - \boldsymbol{\mu}_{PE_i}) - \frac{1}{2}\ln|\boldsymbol{\Sigma}_{PE_i}|, \tag{6.10}$$

respectively, where $\boldsymbol{\mu}_{PA_i}$ and $\boldsymbol{\mu}_{PE_i}$ denote the vectors with mean values, and $\boldsymbol{\Sigma}_{PE_i}$ and $\boldsymbol{\Sigma}_{PA_i}$ denote the covariance matrices of the data. A leave-one-out strategy was employed to evaluate classification performance. Hence, the statistical parameters $\boldsymbol{\mu}_{PA_i}$, $\boldsymbol{\mu}_{PE_i}$, $\boldsymbol{\Sigma}_{PE_i}$, and $\boldsymbol{\Sigma}_{PA_i}$ were estimated based on the 10-s segments of all recordings except one; the 10-s segments of the remaining recording were used to test classification performance. The leave-one-out strategy was repeated until all recordings had been used as test data; the overall performance figure was obtained by averaging the individual results.

Assuming that persistent and paroxysmal AF occur with equal prior probabilities, the feature vector $\mathbf{y}_{i,l}$ was classified as paroxysmal AF if

$$g_i(\mathbf{y}_{i,l}) = g_{PA_i}(\mathbf{y}_{i,l}) - g_{PE_i}(\mathbf{y}_{i,l}) > \epsilon, \tag{6.11}$$

and otherwise as persistent AF. Obviously, this classifier can be optimized for paroxysmal AF at the expense of persistent AF by tuning the threshold ϵ, and vice versa.

The average classification rates for PA and PE are presented in Table 6.4 for $\epsilon = 0$. It is obvious that PA segments are more accurately classified than are those with PE. The average classification rate improved for PE when information on harmonics was added, increasing from 93.9% to 96.5% and 95.8% depending on if $\mathcal{S}_1$ and $\mathcal{S}_2$ or a was added, however, the already high rate for PA (99.6%) did not improve.

Table 6.4: Average classification rate as percentage of correctly classified 10-s segments on a patient basis, expressed as median and interquartile range.

Feature vector	Paroxysmal AF	Persistent AF
$\mathbf{y}_1$	99.6 (99.4–100)	93.9 (51.8–99.3)
$\mathbf{y}_2$	98.7 (88.2–100)	96.5 (57.0–99.2)
$\mathbf{y}_3$	99.3 (91.9–100)	95.8 (61.1–98.7)
$\mathbf{y}_4$	99.0 (91.6–100)	91.9 (42.7–98.2)

The region of convergence (ROC) curves that resulted from the classifiers based on $\mathbf{y}_1$, $\mathbf{y}_2$, $\mathbf{y}_3$, and $\mathbf{y}_4$ are presented in Fig. 6.6. Each curve was obtained by averaging the results from all 10-s segments of each patient group. The three classifiers based on sample entropy performed better than did the classifier based on f_0. The best performance in terms of area under the ROC curve (AROC) was obtained with $\mathbf{y}_3$.

The study shows that short segments with paroxysmal and persistent AF can be classified with good accuracy in ambulatory recordings. The sample entropy of the dominant atrial frequency subband, combined with the relative harmonics energy, was found to produce an AROC which was superior to classification based on the dominant atrial frequency only. Considering the highly variable signal quality of an ambulatory recording, it can be concluded that the proposed signal processing techniques offer a robust approach to the analysis of atrial activity in the surface ECG.

6.5 Paper V: Model Based Analysis of the Ventricular Response during Atrial Fibrillation

The aim of this study is to develop an AV model whose parameters can be estimated from the ECG. Our model incorporates the concepts of dual AV nodal paths, relative refractoriness, and concealed conduction. Information contained in the RR series as well as in the atrial activity of the ECG are combined to find the optimal model parameters, using maximum likelihood estimation. Thus, a set of parameters related to the electrophysiological characteristics of the AV

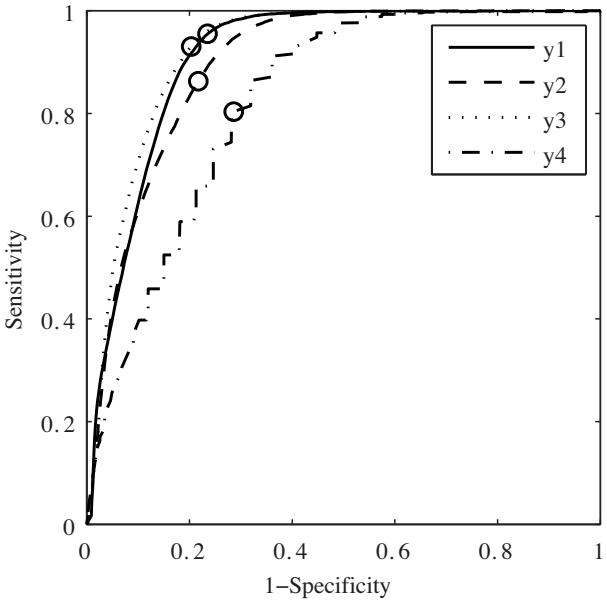

Figure 6.6: ROC curves for AF classifiers based on different feature vectors. The performance for $\epsilon = 0$ is marked with "o". The area under the ROC (AROC) equals 0.913, 0.900, 0.923, and 0.826 for $\mathbf{y}_1$, $\mathbf{y}_2$, $\mathbf{y}_3$, and $\mathbf{y}_4$, respectively.

node can be obtained for each analyzed signal.

In this model, atrial impulses are assumed to arrive to the AV node according to a Poisson process with mean arrival rate λ. Each atrial impulse results in a ventricular contraction unless it is blocked at the AV node; the probability of an atrial impulse being blocked $\beta(t)$, is dependent on the time elapsed since the previous ventricular activation t.

Atrial impulses are blocked when the cells of the AV node are refractory. The refractory period consists of a deterministic part τ, and a stochastic prolongation τ_p modeling concealed conduction and relative refractoriness. The length of the extended refractory period is assumed to be uniformly distributed in the interval $[0, \tau_p^{max}]$. Hence, all atrial impulses arriving at the AV node before the end of the refractory period τ are blocked, no impulses arriving after the end of the maximally extended refractory period $\tau + \tau_p^{max}$ are blocked, and the likelihood of an atrial impulse being blocked between τ and $\tau + \tau_p^{max}$ is assumed to be linearly decreasing.

The deterministic part of the refractory period can take on two different values, τ_1 and τ_2, corresponding to dual AV nodal paths. The maximal prolongation τ_p^{max} is assumed to be equal for the two paths. Hence, the probability of an atrial impulse being blocked in the two paths paths is given by $\beta_1(t)$ and $\beta_2(t)$, respectively, where

$$\beta_i(t) = \begin{cases} 1, & t < \tau_i \\ 1 - \dfrac{t - \tau_i}{\tau_p^{max}}, & \tau_i < t < \tau_i + \tau_p^{max}, \quad i = 1, 2 \\ 0, & t > \tau_i + \tau_p^{max}. \end{cases} \tag{6.12}$$

The probability of an atrial impulse taking the path corresponding to the shortest refractory period τ_1 is given by α. Hence, the probability of an atrial impulse being blocked, denoted $\beta(t)$, is given by $\beta_1(t)$ and $\beta_2(t)$,

$$p(\beta(t) = \beta_i(t)) = \begin{cases} \alpha, & i = 1 \\ 1 - \alpha, & i = 2. \end{cases} \tag{6.13}$$

Using this model, a PDF of the RR interval lengths x can be derived,

$$p_x(x) = \alpha p_{x,1}(x) + (1 - \alpha) p_{x,2}(x), \tag{6.14}$$

where

$$p_{x,i}(x) = \begin{cases} 0, & x < \tau_i \\ \dfrac{\lambda(x - \tau_i)}{\tau_p^{max}} \exp\left\{ \dfrac{\lambda(x - \tau_i)^2}{2\tau_p^{max}} \right\}, & \tau_i < x < \tau_i + \tau_p^{max}, \quad i = 1, 2 \\ \lambda \exp\left\{ \dfrac{\lambda \tau_p^{max}}{2} - \lambda(x - \tau_i - \tau_p^{max}) \right\}, & x > \tau_i + \tau_p^{max}. \end{cases} \tag{6.15}$$

Since ventricular activations are triggered according to a Poisson process, the time intervals between consecutive ventricular activations are independent. Hence, the joint probability of an RR series is given by

$$\begin{aligned} p_x(x_1, x_2, \ldots x_M) &= \prod_{m=1}^{M} p_x(x_m) \\ &= \prod_{m=1}^{M} (\alpha p_{x,1}(x_m) + (1 - \alpha) p_{x,2}(x_m)), \end{aligned} \tag{6.16}$$

where $p_{x,1}(x_m)$ and $p_{x,2}(x_m)$ are given by (6.15).

A functional dependence of the deterministic part of the refractory period τ on the previous RR interval is included in the model, such that a longer RR interval is followed by a longer refractory period,

$$\tau_{i,m} = \tau_i^{min} + s_\tau d_{RR,m-1}, \quad i = 1, 2. \tag{6.17}$$

where τ_i^{min} and s_τ defines the linear dependence, and $\tau_{i,m}$ denotes the refractory period following the m:th ventricular activation. The magnitude of the linear dependence s_τ is assumed to be equal for τ_1 and τ_2, so that the difference between the two refractory periods $\Delta\tau$ is constant.

$$\begin{aligned} \tau_{2,m} &= \tau_2^{min} + s_\tau d_{RR,m-1} \\ &= \tau_1^{min} + s_\tau d_{RR,m-1} + \Delta\tau \\ &= \tau_{1,m} + \Delta\tau \end{aligned} \tag{6.18}$$

Estimation of model parameters from ECG signals is based on the detected RR series as well as on the atrial activity; the arrival rate of atrial impulses to the AV node λ is estimated by the dominant AF frequency. The parameters defining the functional refractory period, s_τ and τ_1^{min}, are obtained from the lower envelope of the Poincaré plot of the RR series.

The model parameters

$$\boldsymbol{\theta} = \begin{bmatrix} \alpha \\ \Delta\tau \\ \tau_p^{max} \end{bmatrix}, \tag{6.19}$$

related to the dual AV nodal paths and prolongation of the refractory period, are estimated by maximizing the joint probability $p_x(x_1, x_2, \ldots x_M)$ given in (6.16). However, in order to reduce the dependences of consecutive RR intervals $x'_1, x'_2, \ldots x'_M$ the following simple transformation is used

$$x_m = x'_m - s_\tau x'_{m-1}. \tag{6.20}$$

The number of RR intervals required for accurate estimation was tested using simulated RR series; for most parameter settings, less than 500 RR intervals were required for the estimates to converge. The model was evaluated on consecutive 30-min segments of Holter-ECG signals from 40 patients with AF. A measure of model fit $\mathcal{U}$ based on the joint area of the estimated model PDF and an empirical PDF estimated using wavelet-based density estimation [103] was computed; the mean value of fit was $\mathcal{U} = 84.4 \pm 5.1\%$. In 85.7% of the analyzed 30-min segments (1729 out of 2018), $\mathcal{U} > 80\%$ which in this study is considered as a sufficiently accurate model fit.

An example of two PDFs from 30-min segments from the same patient are displayed in Figs. 6.7(b) and (c). In these examples, $\mathcal{U} = 92.6\%$ and 90.9%,

respectively. The trends of the estimated model parameters over 24 h are displayed in Fig. 6.7(a). For this patient, a decrease in λ is associated with an increase in τ_1^{min}, a decrease in α and a slight increase in τ_p^{max}. This result suggests that the refractory period of both AV nodal paths increases, that the probability of conduction through the path with the shorter refractory period decreases, and that there is an extended prolongation of the refractory periods.

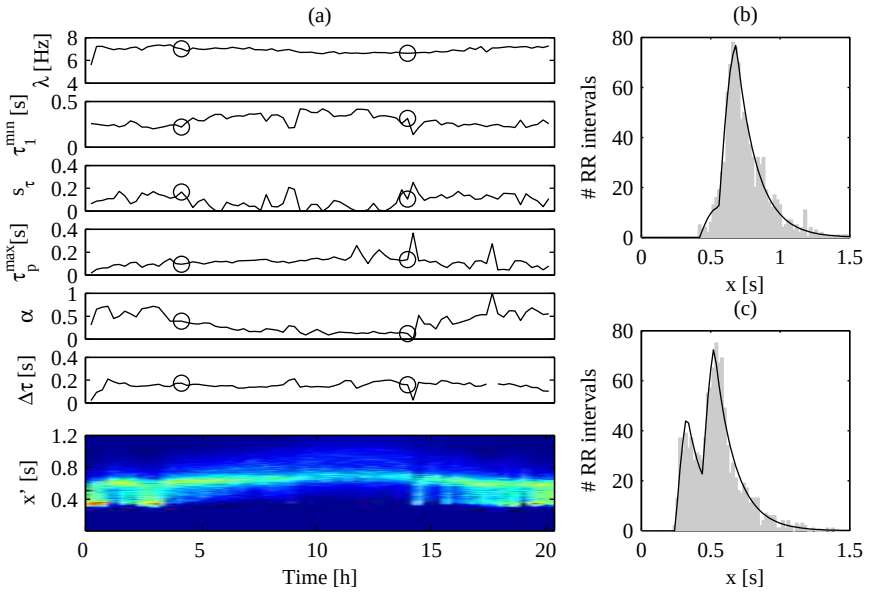

Figure 6.7: (a) Trends of estimated model parameters and sequential RR interval histograms from a patient with sustained AF. The PDFs corresponding to the encircled parameters are displayed in (b) and (c), respectively. Since $\alpha = 1$, $\Delta\tau$ presents an undefined value at $t = 18$ h.

Figure 6.8 displays an example with RR interval histograms, Poincaré plots and estimated model PDFs during a head-up tilt test. The atrial activity and ventricular response are altered when the patient is tilted; the atrial rate λ increases, while the RR intervals are shorter due to increase in α, and decrease in $\Delta\tau$ and τ_1^{min}. This suggests that the refractory period of both AV nodal paths decreases, the longer one more than the shorter one, and that the probability of conduction through the path with the shorter refractory period increases.

In conclusion, our model of AV nodal function during AF, which incorpo-

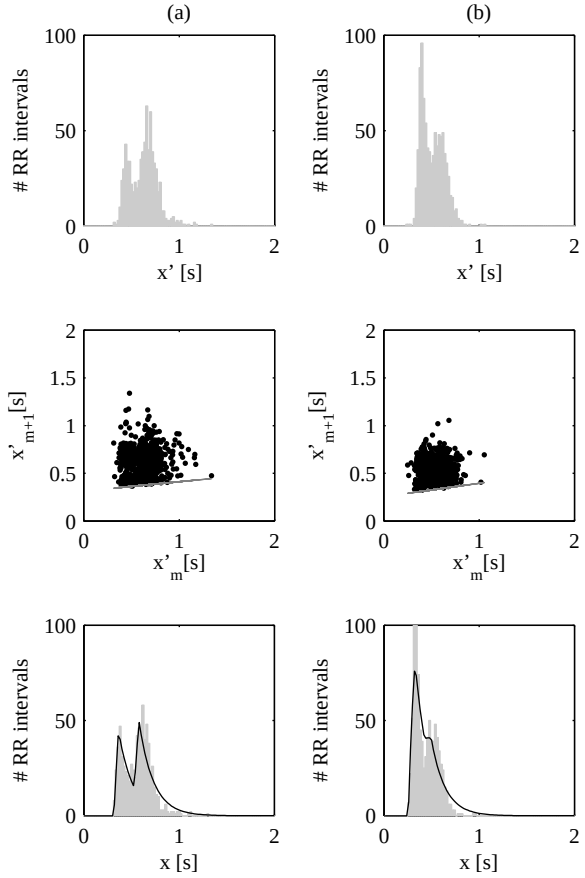

Figure 6.8: (top) Histogram of x', (middle) Poncaré plot of x' with estimated lower envelope, and (bottom) histogram of x with corresponding estimated model PDF from the same patient during (a) rest and (b) head-up tilt. (a) Fit: $\mathcal{U} = 84.8\%$. Estimated parameter values: $\hat{\lambda} = 6.6$ Hz, $\hat{\tau}_1^{min} = 0.31$ s, $\hat{s}_\tau = 0.10$, $\hat{\alpha} = 0.54$, $\hat{\Delta}\tau = 0.22$ s and $\hat{\tau}_p^{max}$=0.05 s. (b) Fit: $\mathcal{U} = 82.3\%$. Estimated parameter values: $\hat{\lambda} = 6.9$ Hz, $\hat{\tau}_1^{min} = 0.26$ s, $\hat{s}_\tau = 0.14$, $\hat{\alpha} = 0.84$, $\hat{\Delta}\tau = 0.17$ s and $\hat{\tau}_p^{max}$=0.07 s.

rates the concepts of dual AV nodal paths, concealed conduction and relative refractoriness, can represent a wide variety of RR interval distributions, and the model parameters can be accurately estimated from ECGs.

References

[1] L. Sörnmo and P. Laguna, *Bioelectrical Signal Processing in Cardiac and Neurological Applications*. Amsterdam: Elsevier, 2005.

[2] V. Fuster, L. E. Rydén, D. S. Cannom, H. J. Crijns, A. B. Curtis, K. A. Ellenbogen, *et al.*, "ACC/AHA/ESC 2006 guidelines for the management of patients with atrial fibrillation: A report of the American College of Cardiology/American Heart Association task force on practice guidelines and the European Society of Cardiology committee for practice guidelines," *Circulation*, vol. 114, pp. e257–e354, Aug 2006.

[3] G. Moe, "On the multiple wavelet hypothesis of atrial fibrillation," *Arch. Int. Pharmacodyn. Ther.*, vol. 140, pp. 183–188, 1962.

[4] S. Nattel, "New ideas about atrial fibrillation 50 years on," *Nature*, vol. 415, pp. 219–226, 2002.

[5] R. Langendorf, A. Pick, and L. Katz, "Ventricular response in atrial fibrillation: Role of concealed conduction in the AV junction," *Circulation*, vol. 32, pp. 69–75, 1965.

[6] S. Garrigue, P. Tchou, and T. Mazgalev, "Role of the differential bombardment of atrial inputs to the atrioventricular node as a factor influencing ventricular rate during high atrial rate," *Cardiovasc. Res.*, vol. 44, pp. 344–355, 1999.

[7] G. Wagner, *Practical Electrocardiography*. Williams & Wilkins, 9 ed., 1994.

[8] S. Nattel and L. Opie, "Controversies in cardiology 3: Controversies in atrial fibrillation," *Lancet*, vol. 367, pp. 262–72, 2006.

[9] S. Al-Khatib, W. Wilkinson, L. Sanders, E. McCarthy, and E. Pritchett, "Observations on the transition from intermittent to permanent atrial fibrillation," *Am. Heart J.*, vol. 140, pp. 142–145, July 2000.

[10] S. Mittal, K. Stein, S. Markowitz, A. Guttigoli, and B. Lerman, "An update on electrical cardioversion of atrial fibrillation," *Card. Electrophysiol. Rev.*, vol. 7, pp. 285–289, 2003.

[11] G. Boriani, M. Biffi, and I. Diemberger, "Rate control in atrial fibrillation: Choice of treatment and assessment of efficacy.," *Drugs*, vol. 63, pp. 1489–1510, 2003.

[12] G. Lip and S. Kamath, "Atrial fibrillation (2): Antiarrhythmic agents," *The Pharmaceutical Journal*, vol. 264, pp. 659–663, 2000.

[13] J. Burkhardt and A. Natale, "New technologies in atrial fibrillation ablation.," *Circulation*, vol. 120, pp. 1533–1541, 2009.

[14] H. Calkins, J. Brugada, D. Packer, R. Cappato, S.-A. Chen, H. Crijns, *et al.*, "HRS/EHRA/ECAS expert consensus statement on catheter and surgical ablation of atrial fibrillation: Recommendations for personnel, policy, procedures and follow-up," *Heart Rhythm*, vol. 4, pp. 816–861, 2007.

[15] J. Slocum, E. Byrom, L. McCarthy, A. Sahakian, and S. Swiryn, "Computer detection of atrioventricular dissociation from surface electrocardiograms during wide QRS complex tachycardia," *Circulation*, vol. 72, pp. 1028–1036, 1985.

[16] M. Stridh and L. Sörnmo, "Spatiotemporal QRST cancellation techniques for analysis of atrial fibrillation," *IEEE Trans. Biomed. Eng.*, vol. 48, pp. 105–111, 2001.

[17] F. Castells, C. Mora, and J. J. Rieta, "Estimation of atrial fibrillatory wave from single-lead atrial fibrillation electrocardiograms using principal component analysis concepts.," *Med. Biol. Eng. Comp.*, vol. 43, pp. 557–561, 2005.

[18] M. Lemay, J. Vesin, A. van Oosterom, V. Jaquement, and L. Kappenberger, "Cancellation of ventricular activity in the ECG: Evaluation of novel and existing methods," *IEEE Trans. Biomed. Eng.*, vol. 54, pp. 542–546, 2007.

[19] R. Alcaraz and J. J. Rieta, "Adaptive singular value cancelation of ventricular activity in single-lead atrial fibrillation electrocardiograms," *Physiol. Meas.*, vol. 29, pp. 1351–1369, 2008.

[20] D. Raine, P. Langley, A. Murray, S. Furniss, and J. Bourke, "Surface atrial frequency analysis in patients with atrial fibrillation: Assessing the effects of linear left atrial ablation," *J Cardiovasc Electrophysiol*, vol. 16, pp. 838–844, 2005.

[21] J. J. Rieta, F. Castells, V. Zarzoso, and J. Millet, "Atrial activity extraction for atrial fibrillation analysis using blind source separation," *IEEE Trans. Biomed. Eng.*, vol. 51, pp. 1176–1186, 2004.

[22] F. Castells, J. J. Rieta, J. Millet, and V. Zarzoso, "Spatiotemporal blind source separation approach to atrial activity estimation in atrial tachyarrhythmias," *IEEE Trans. Biomed. Eng.*, vol. 52, pp. 258–267, 2005.

[23] C. Vayá, J. J. Rieta, C. Sanchez, and D. Moratal, "Convolutive blind source separation algorithms applied to the electrocardiogram of atrial fibrillation: Study of performance," *IEEE Trans. Biomed. Eng.*, vol. 54, pp. 1530–1533, 2007.

[24] G. Wang, N. Rao, S. J. Shepherd, and C. B. Beggs, "Extraction of desired signal based on AR model with its application to atrial activity estimation in atrial fibrillation," *EURASIP Journal on Advances in Signal Processing*, vol. 2008, 2008.

[25] V. Zarzoso and P. Comon, "Robust independent component analysis by iterative maximization of the kurtosis contrast with algebraic optimal step size," *IEEE Trans. Neural Networks*, vol. 21, pp. 248–261, 2010.

[26] F. Castells, P. Laguna, L. Sörnmo, A. Bollmann, and J. M. Roig, "Principal component analysis in ECG signal processing," *EURASIP Journal on Advances in Signal Processing*, vol. 2007, 2007.

[27] A. Hyvarinen, J. Karhunen, and E. Oja, *Independent Component Analysis*. Wiley Interscience, 2001.

[28] P. Langley, J. J. Rieta, M. Stridh, J. Millet, L. Sörnmo, and A. Murray, "Comparison of atrial signal extraction algorithms in 12-lead ECGs with atrial fibrillation," *IEEE Trans. Biomed. Eng.*, vol. 53, pp. 343–346, 2006.

[29] V. Jaquement, A. van Oosterom, J. Vesin, and L. Kappenberger, "Analysis of elactrocardiograms during atrial fibrillation," *IEEE EMB Magazine*, vol. 25, pp. 79–88, 2006.

[30] M. Stridh, L. Sörnmo, C. Meurling, and B. Olsson, "Time-dependent spectral properties in atrial fibrillation signals," *IEEE Trans. Biomed. Eng.*, pp. 19–27, 2001.

[31] M. Stridh, L. Sörnmo, C. Meurling, and S. Olsson, "Sequential characterization of atrial tachyarrhythmias based on ECG time–frequency analysis," *IEEE Trans. Biomed. Eng.*, vol. 51, pp. 100–114, 2004.

[32] M. Lemay, Y. Prudat, V. Jacquemet, and J.-M. Vesin, "Phase-rectified signal averaging used to estimate the dominant frequencies in ECG signals during atrial fibrillation," *IEEE Trans. Biomed. Eng.*, vol. 55, pp. 2538–2547, 2008.

[33] M. Stridh, D. Husser, A. Bollmann, and L. Sornmo, "Waveform characterization of atrial fibrillation using phase information," *IEEE Trans. Biomed. Eng.*, vol. 56, pp. 1081–1089, 2009.

[34] R. Alcaraz and J. J. Rieta, "A review on sample entropy applications for the non-invasive analysis of atrial fibrillation electrocardiograms," *Biomedical Signal Processing and Control*, vol. 5, pp. 1–14, 2010.

[35] F. Nilsson, M. Stridh, A. Bollmann, and L. Sörnmo, "Predicting spontaneous termination of atrial fibrillation using the surface ECG," *Med. Eng. Physics*, vol. 28, pp. 802–808, 2006.

[36] J. Ng, A. Sahakian, W. Fisher, and S. Swiryn, "Surface ECG vector characteristics of organized and disorganized atrial activity during atrial fibrillation," *J. Electrocardiol.*, vol. 37, pp. 91–97, 2004.

[37] U. Richter, M. Stridh, A. Bollmann, D. Husser, and L. Sornmo, "Spatial characteristics of atrial fibrillation electrocardiograms," *J. Electrocardiol.*, vol. 41, pp. 165–172, 2008.

[38] P. Bonizzi, M. Guillem, A. M. Climent, J. Millet, V. Zarzoso, F. Castells, and O. Meste, "Noninvasive assessment of the complexity and stationarity of the atrial wavefront patterns during atrial fibrillation," *IEEE Trans. Biomed. Eng.*, vol. 57, pp. 2147–2157, 2010.

[39] M. Holm, S. Pehrsson, M. Ingemansson, L. Sörnmo, R. Johansson, L. Sandhall, M. Sunemark, B. Smideberg, C. Olsson, and S. B. Olsson, "Non-invasive assessment of atrial refractoriness during atrial fibrillation in man—introducing, validating and illustrating a new ECG method," *Cardiovasc. Res.*, vol. 38, pp. 69–81, 1998.

[40] A. Bollmann, N. Kanuru, K. McTeague, P. Walter, D. B. DeLurgio, and J. Langberg, "Frequency analysis of human atrial fibrillation using the surface electrocardiogram and its response to ibutilide," *Am. J. Cardiol.*, vol. 81, pp. 1439–1445, 1998.

[41] D. Husser, M. Stridh, D. S. Cannom, A. K. Bhandari, M. J. Girsky, S. Kang, L. Sörnmo, S. B. Olsson, and A. Bollmann, "Validation and clinical application of time–frequency analysis of atrial fibrillation electrograms," *J. Cardiovasc. Electrophysiol.*, vol. 18, pp. 41–46, 2007.

[42] D. Husser, M. Stridh, L. Sornmo, C. Geller, H. Klein, S. Olsson, and A. Bollmann, "Time-frequency analysis of the surface electrocardiogram for monitoring antiarrhythmic drug effects in atrial fibrillation," *Am. J. Cardiol.*, vol. 95, pp. 526–528, 2005.

[43] Q. Xi, A. V. Sahakian, T. G. Frohlich, J. Ng, and S. Swiryn, "Relationship between patterns of occurrence of atrial fibrillation and surface electrocardiographic fibrillatory wave characteristics," *Heart Rhythm*, vol. 1, pp. 656–663, 2004.

[44] A. Bollmann, K. Binias, I. Toepffer, J. Molling, C. Geller, and H. Klein, "Importance of left atrial diameter and atrial fibrillatory frequency for conversion of persistent atrial fibrillation with oral flecainide," *Am. J. Cardiol.*, vol. 90, pp. 1011–1014, 2002.

[45] J. Langberg, J. Brunette, and K. McTeague, "Spectral analysis of the electrocardiogram predicts recurrence of atrial fibrillation after cardioversion," *J. Electrocardiol.*, vol. 31, pp. 80–84, 1998.

[46] A. Bollmann, D. Husser, L. Mainardi, F. Lombardi, P. Langley, A. Murray, J. J. Rieta, J. Millet, S. B. Olsson, M. Stridh, and L. Sörnmo, "Analysis of surface electrocardiograms in atrial fibrillation: Techniques, research, and clinical applications," *Europace*, vol. 8, pp. 911–926, 2006.

[47] A. Bollmann, K. Sonne, H. Esperer, I. Toepffer, and H. Klein, "Circadian variations in atrial fibrillatory frequency in persistent human atrial fibrillation," *PACE*, vol. 23, pp. 1867–1871, 2000.

[48] C. Meurling, J. Waktare, F. Holmqvist, A. Hedman, A. Camm, S. Olsson, and M. Malik, "Diurnal variations of the dominant cycle length of chronic atrial fibrillation," *Am. J. Physiol.*, vol. 280, pp. H401–H406, 2001.

[49] F. Sandberg, A. Bollmann, D. Husser, M. Stridh, and L. Sörnmo, "Circadian variation in dominant atrial fibrillation frequency in persistent atrial fibrillation," *Physiol. Meas.*, vol. 31, pp. 531–542, 2010.

[50] A. Bollmann, K. Wodarz, H. Esperer, I. Toepffer, and H. Klein, "Response of atrial fibrillatory activity to carotide sinus massage in patients with atrial fibrillation," *PACE*, vol. 24, pp. 1363–1368, 2001.

[51] M. Ingemansson, M. Holm, and S. B. Olsson, "Autonomic modulation of the atrial cycle length by the head up tilt test: Non-invasive evaluation in patients with chronic atrial fibrillation," *Heart*, vol. 80, pp. 71–76, 1998.

[52] F. Holmqvist, M. Stridh, J. Waktare, J. Brandt, L. Sörnmo, and C. Meurling, "Rapid fluctuations in atrial fibrillatory electrophysiology detected during controlled respiraiton," *Am. J. Physiol. Heart Circ. Physiol.*, vol. 289, pp. H754–H760, 2005.

[53] S. Kodituwakku, R. Kennedy, and T. Abhayapala, "Radial function based kernel design for time-frequency distributions," *IEEE Trans. Signal Proc.*, vol. 58, pp. 3395–3400, 2010.

[54] D. Husser, D. S. Cannom, A. K. Bhandari, M. Stridh, L. Sörnmo, S. B. Olsson, and A. Bollmann, "Electrocardiographic characteristics of fibrillatory waves in new-onset atrial fibrillation," *Europace*, vol. 9, pp. 638–642, 2007.

[55] F. Holmqvist, M. Stridh, J. E. P. Waktare, A. Roijer, L. Sörnmo, P. G. Platonov, and C. J. Meurling, "Atrial fibrillation signal organization predicts sinus rhythm maintenance in patients undergoing cardioversion of atrial fibrillation," *Europace*, vol. 8, pp. 559–565, 2006.

[56] V. Corino, L. Mainardi, M. Stridh, and L. Sörnmo, "Improved time–frequency analysis of atrial fibrillation signals using spectral modeling," *IEEE Trans. Biomed. Eng.*, vol. 55, pp. 2723–2730, 2008.

[57] L. Mainardi, M. Matteucci, and R. Sassi, "On predicting the spontaneous termination of atrial fibrillation episodes using linear and nonlinear parameters of ECG signal and RR series," in *Proc. Computers in Cardiology*, pp. 665–668, 2004.

[58] L. Mainardi, A. Porta, G. Calcagnini, P. Bartolini, A. Michelucci, and S. Cerutti, "Linear and non-linear analysis of atrial signals and local activation period series during atrial-fibrillation episodes," *Med. Biol. Eng. Comput.*, vol. 39, pp. 249–254, 2001.

[59] S. J. Richman and J. R. Moorman, "Physiological time-series analysis using approximate entropy and sample entropy," *Am. J. Physiol.*, vol. 278, pp. H2039–H2049, 2000.

[60] S. M. Pincus, "Approximate entropy as a measure of system complexity," *Proc. Natl. Acad. Sci. USA*, vol. 88, pp. 2297–2301, 1991.

[61] R. Alcaraz and J. J. Rieta, "Wavelet bidomain sample entropy analysis to predict spontaneous termination of atrial fibrillation," *Physiol. Meas.*, vol. 29, pp. 65–80, 2008.

[62] R. Alcaraz and J. J. Rieta, "A non-invasive method to predict electrical cardioversion outcome of persistent atrial fibrillation," *Med. Biol. Eng. & Comput.*, vol. 46, pp. 625–635, 2008.

[63] R. Alcaraz and J. J. Rieta, "Sample entropy of the main atrial wave predicts spontaneous termination of paroxysmal atrial fibrillation," *Med. Eng. Phys.*, vol. 31, pp. 917–922, 2009.

[64] R. Alcaraz and J. J. Rieta, "The application of nonlinear metrics to assess organization differences in short recordings of paroxysmal and persistent atrial fibrillation," *Physiol. Meas.*, vol. 31, pp. 115–130, 2010.

[65] P. Macfarlane, L. E. L, and O. Pahlm, *12-Lead vectorcardiography.* Butterworth-Heinemann, 1995.

[66] S. Dibs, J. Ng, R. Arora, R. Passman, A. Kadish, and J. Goldberger, "Spatiotemporal characterization of atrial activation in persistent human atrial fibrillation: Multisite electrogram analysis and surface electrocardiographic correlations—a pilot study," *Heart Rhythm*, vol. 5, pp. 686 – 693, 2008.

[67] R. J. Cohen, R. D. Berger, and T. Dushane, "A quantitative model for the ventricular response during atrial fibrillation," *IEEE Trans. Biomed. Eng.*, vol. 30, pp. 769–781, 1983.

[68] S. Rokas, S. Gaitanidou, S. Chatzidou, C. Pamboucas, D. Achtipis, and S. Stamatelopoulos, "Atrioventricular node modification in patients with chronic atrial fibrillation: Role of morphology of RR interval variation," *Circulation*, vol. 103, pp. 2942–2948, 2001.

[69] S. Rokas, S. Gaitanidou, S. Chatzidou, N. Agrios, and S. Stamatelopoulos, "A noninvasive method for the detection of dual atrioventricular node physiology in chronic atrial fibrillation," *Am. J. Cardiol.*, vol. 84, pp. 1442–1445, 1999.

[70] S. B. Olsson, N. Cai, M. Dohnal, and K. Talwar, "Noninvasive support for and characterization of multiple pathways in patients with mitral valve disease and atrial fibrillation," *Eur. Heart J.*, vol. 7, pp. 320–333, 1986.

[71] M. Ingemansson, J. Carlson, and S. Olsson, "Modification of intrinsic AV-nodal properties by magnesium in combination with glucose, insulin, and potassium (gik) during chronic atrial fibrillation," *J Electrocardiol*, vol. 31, pp. 281–292, 1998.

[72] J. Tebbenjohanns, B. Schumacher, T. Korte, M. Niehaus, and D. Pfeiffer, "Bimodal RR interval distribuiton in chronic atrial fibrillation," *J. Cardiovasc. Electrophysiol.*, vol. 11, pp. 497–503, 2000.

[73] N. Cai, M. Dohnal, and S. B. Olsson, "Methodological aspects of the use of heart rate stratified RR interval histograms in the analysis of atrioventricular conduction during atrial fibrillation," *Cardiovasc. Res.*, vol. 21, pp. 455–462, 1987.

[74] V. Corino, A. Climent, L. Mainardi, and A. Bollmann, "Analysis of ventricular response during atrial fibrillation," in *Understanding Atrial Fibrillaiton: The Signal Processing Contribution* (L. Mainardi, L. Sörnmo, and S. Cerutti, eds.), Morgan & Claypool, 2008.

[75] J. Billette, R. Nadeau, and F. Roberge, "Relation between the minimum RR interval during atrial fibrillation and the functional refrectory period of the AV junction," *Cardiovasc. Res.*, vol. 8, pp. 347–351, 1974.

[76] J. Hayano, S. Sakata, A. Okada, S. Mukai, and T. Fujinami, "Circadian rhythms of atrioventricular conduction properties in chronic atrial fibrillation with and without heart failure – relation between mean heart rate and measures of heart rate variability," *J Am Coll Cardiol*, vol. 31, pp. 158–166, 1998.

[77] A. Climent, M. Guillem, D. Husser, F. Castells, J. Millet, and A. Bollmann, "Circadian rhythm of ventricular response during atrial fibrillation is not determined by dual atrioventricular nodal pathway conduction," *J. Electrocardiol.*, vol. 40, p. S30, 2007.

[78] M. van den Berg, T. van Noord, J. Brouwer, J. Haaksma, D. van Veldhuisen, H. Crijns, and I. V. Gelder, "Clustering of RR intervals predicts effective electrical cardioversion for atrial fibrillation," *J. Cardiovasc. Electrophysiol.*, vol. 15, pp. 1027–1033, 2004.

[79] A. Climent, M. de la Salud Guillem, D. Husser, F. Castells, J. Millet, and A. Bollmann, "Poincaré surface profiles of RR intervals: A novel noninvasive method for the evaluation of preferential AV nodal conduction during atrial fibrillation," *IEEE Trans. Biomed. Eng.*, vol. 56, pp. 433–442, 2009.

[80] P. Jørgensen, C. Schäfer, P. Guerra, M. Talajic, S. Nattel, and L. Glass, "A mathematical model of human atrioventricular nodal function incorporating concealed conduction," *Bull Math Biol*, vol. 64, pp. 1083–1099, 2002.

[81] L. Mangin, A. Vinet, P. Page, and L. Glass, "Effects of antiarrhythmic drug therapy on atrioventricular nodal function during atrial fibrillation in humans," *Europace*, vol. 7, pp. S71–S82, 2005.

[82] A. Rashidi and I. Khodarahmi, "Nonlinear modeling of the atrioventricular node physiology in atrial fibrillation," *Journal of Theoretical Biology*, vol. 232, pp. 545 – 549, 2005.

[83] J. Lian, D. Müssig, and V. Lang, "Computer modeling of ventricular rhythm during atrial fibrillation and ventricular pacing," *IEEE Trans. Biomed. Eng.*, vol. 53, pp. 1512–1520, 2006.

[84] J. Lian and D. Müssig, "Heart rhythm and cardiac pacing: An integrated dual-chamber heart and pacer model," *Ann. Biomed. Eng.*, vol. 37, pp. 64–81, 2009.

[85] A. L. Goldberger, L. A. N. Amaral, L. Glass, J. M. Hausdorff, P. C. Ivanov, R. G. Mark, J. E. Mietus, G. B. Moody, C.-K. Peng, and H. E. Stanley, "PhysioBank, PhysioToolkit, and PhysioNet: Components of a new research resource for complex physiologic signals," *Circulation*, vol. 101, pp. e215–e220, 2000.

[86] G. B. Moody, "Spontaneous termination of atrial fibrillation: A challenge from PhysioNet and Computers in Cardiology 2004," in *Proc. Comput. Cardiol.*, vol. 31, pp. 101–104, IEEE Press, 2004.

[87] I. A. Rezek and S. J. Roberts, "Stochastic complexity measures for physiological signal analysis," *IEEE Trans. Biomed. Eng.*, vol. 45, pp. 1186–1191, 1998.

[88] L. Rabiner and B. H. Juang, "An introduction to hidden Markov models," *IEEE ASSP Magazine*, pp. 4–19, 1986.

[89] G. D. Forney, "The Viterbi algorithm," *IEEE Proc.*, vol. 61, pp. 268–278, 1973.

[90] F. Sandberg, M. Stridh, and L. Sörnmo, "Frequency tracking of atrial fibrillation using hidden Markov models," *IEEE Trans. Biomed. Eng.*, vol. 55, pp. 502–511, 2008.

[91] C. Bingham, B. Arbogast, G. C. Guillaumc, J. K. Lee, and F. Halberg, "Inferential statistical methods for estimating and comparing cosinor parameters," *Chronobiologia*, vol. 9, pp. 397–439, 1982.

[92] M. Tabata, T. Takeshima, N. Burioka, T. Nomura, K. Ishizaki, N. Mori, *et al.*, "Cosinor analysis of heart rate variability in ambulatory migraineurs," *Headache*, vol. 40, pp. 457–463, 2000.

[93] J. Fernández, R. Hermida, and A. Mojón, "Chronobiological analysis techniques. Application to blood pressure," *Phil. Trans. R. Soc. A*, vol. 367, pp. 431–445, 2009.

[94] M. A. Watanabe, M. Alford, R. Schneider, A. Bauer, P. Barthel, P. K. Stein, and G. Schmidt, "Demonstration of circadian rhythm in heart rate turbulence using novel application of correlator functions," *Heart Rhythm*, vol. 4, pp. 292–300, 2007.

[95] R. Atarius and L. Sörnmo, "Cardiac late potentials and signal-to-noise ratio enhancement by ensemble correlation," *IEEE Trans. Biomed. Eng.*, vol. 42, pp. 1132–1137, 1995.

[96] F. Chiarugi, M. Varanini, F. Cantini, F. Conforti, and G. Vrouchos, "Noninvasive ECG as a tool for predicting termination of paroxysmal atrial fibrillation," *IEEE Trans. Biomed. Eng.*, vol. 54, pp. 1399–1406, 2007.

[97] R. Sun and Y. Wang, "Predicting termination of atrial fibrillation based on the structure and quantification of the recurrence plot," *Med. Eng. Phys.*, vol. 30, pp. 1105–1111, 2008.

[98] S. Petrutiu, A. V. Sahakian, J. Ng, and S. Swiryn, "Analysis of the surface electrocardiogram to predict termination of atrial fibrillation: The 2004 Computers in Cardiology/PhysioNet challenge," in *Proc. Comput. Cardiol.*, vol. 31, pp. 105–108, IEEE Press, 2004.

[99] C. Mora, J. Castells, R. Ruiz, J. J. Rieta, J. Millet, C. Sanchez, and S. Morell, "Prediction of spontaneous termination of atrial fibrillation using time–frequency analysis of the atrial fibrillatory wave," in *Proc. Comput. Cardiol.*, vol. 31, pp. 109–112, IEEE Press, 2004.

[100] Q. Xi and S. Shkurovich, "Prediction of spontaneous termination of atrial fibrillation in surface ECG by frequency analysis," in *Proc. Comput. Cardiol.*, vol. 31, pp. 113–116, IEEE Press, 2004.

[101] R. Alcaraz, D. Abásolo, R. Hornero, and J. J. Rieta, "Optimal parameters study for sample entropy-based atrial fibrillation organization analysis," *Comput. Meth. Prog. Biomed.*, vol. 99, pp. 124–132, 2010.

[102] R. Duda, P. Hart, and D. Stork, *Pattern Classification*. New York: John Wiley and Sons, Inc., 2001.

[103] A. Antoniadis and D. T. Pham, "Wavelet regression for random or irregular design," *Computational Statistics and Data Analysis*, vol. 28, pp. 353–369, 1998.